
PERFORM

WP1: Learn and Understand

Knowledge database for understanding the current problems

Deliverable 1.3

Prepared by: GEUS: Lars Kristensen, Knud
 Dideriksen, Hanne Dahl
 Holmslykke, Claus Kjøller and
 Uffe Larsen.
 FT: Troels Mathiesen.
 TNO: Hester Dijkstra, Jonah
 Poort, Laura Wasch, Pejman
 Shoeibi Omrani.
 GFZ: Simona Regenspurg.

Checked by: GEUS: Knud Dideriksen.

Approved by: GEUS: Lars Kristensen.



PERFORM is one of nine projects under the GEOthermica – ERA NET The overarching target of PERFORM is to improve geothermal system performance, lower operational expenses and extend the life-time of infrastructure by the concept of combining data collection, predictive modelling, innovative technology development and in-situ validation. The improvement of geothermal site performance from the proposed work is expected to result in an increase of the energy output by 10 to 50%. In order to reach this goal PERFORM will establish a single and shared knowledge database, build predictive models and demonstrate new and improved, cost-effective technologies which will reduce or even eliminate flow-obstructive scaling, clogging, and resistance to fluid (re-)injection at eight geothermal sites across Europe.



The GEOthermica is supported by the European Union's HORIZON 2020 programme for research, technological development and demonstration under grant agreement No 731117

About PERFORM

Despite years of experience with geothermal systems, the geothermal sector still faces a significant number of underperforming doublets, posing a strong limitation on a region's growth of geothermal energy utilization. A key operational challenge in geothermal energy production is restricted flow. Major obstacles for geothermal flow are scaling (mineral deposition), clogging (solid micro-particle deposition), corrosion and inefficient injection strategies. These issues result in high and mostly unforeseen costs for workovers, and additionally reduce production. In order to overcome these challenges, the consolidation and sharing of knowledge, including validated strategies for prevention and mitigation needs to be in place.

Therefore, a consortium consisting of De Nationale Geologische Onderzoekingen voor Denemark og Grønland (GEUS) and FORCE Technology (FT) from Denmark, Helmholtz Centre Potsdam German Research Centre for Geosciences (GFZ) and Hydroisotop GmbH from Germany and Ammerlaan Geothermie B.V., Greenwell Westland B.V., Wageningen Food & Biobased Research and ECN part of TNO from the Netherlands proposed a GEOTHERMICA project PERFORM, which has been granted. The overarching target of PERFORM is to improve geothermal system performance, lower operational expenses and extend the life-time of infrastructure by the concept of combining data collection, predictive modelling, innovative technology development and in-situ validation. The improvement of geothermal site performance from the proposed work is expected to result in an increase of the energy output by 10 to 50%. In order to reach this goal, PERFORM will establish a single and shared knowledge database, build predictive models and demonstrate new and improved, cost-effective technologies at geothermal sites across Europe.

Based on experiences from geothermal sites within the EU, PERFORM will establish a knowledge database containing information on operational, chemical and physical aspects of geothermal energy production. The database enables sharing experiences from geothermal doublets located in various countries and comparing the performance of different geothermal reservoirs.

PERFORM builds predictive models that allow for pinpointing the most likely sources and causes of failure, as well as the best options for injectivity improvement. The integrated models will provide forecasting for scaling, productivity, and injectivity on short- and long- time scales, supporting early warning and planning of mitigation measures. Coupled thermo-hydro-mechanical-chemical simulators will allow for evaluation of injection temperature that apart for increasing flow will also increase the energy output.

Data and knowledge gathering, and technology demonstration is planned for geothermal sites across Europe. Demonstration of new and improved, cost-effective technologies will allow for the reduction or even elimination of flow-obstructive scaling, clogging, and resistance to fluid (re-)injection. The technologies include low-cost cation extraction filters, self-cleaning particle removal appliances, H₂S removal technology and soft-stimulating injection procedures (thermal and CO₂-injection). The goal is to provide a set of new and improved, low-cost and environmentally friendly technology alternatives.

PERFORM integrates the knowledge database, predictive modelling and advanced technologies into a design and operation toolbox, which will be tied to economical calculations. The toolbox will enable stakeholders and specifically geothermal operators to plan future operations, mitigate existing obstructions, and optimize production/injection procedures, thus ensuring maximum energy production when needed.

This project has been subsidized through the ERANET Cofound GEOTHERMICA (Project no. 731117), from the European Commission, Topsector Energy subsidy from the Ministry of Economic Affairs of the Netherlands, Federal Ministry for Economic Affairs and Energy of Germany and EUDP.

Table of Content

About PERFORM	3
Summary	5
1. Introduction.....	7
2. Data collection	8
2.1 Data from operators of key geothermal sites	8
2.2 Additional data from Dutch sites	10
2.3 New data acquired for Dutch reservoirs	11
2.4 Data collected from the Danish GEOTHERM project.....	12
2.5 Supplementary literature data.....	12
3 The PERFORM database.....	13
4 Website construction	15
5 Analysis of production data	18
5.1 Sønderborg production data	18
5.2 Anomaly detection.....	19
5.2 Predicting missing data	21
6 Analysis of data on water composition	27
6.1 Principal Component Analysis	27
6.2 Correlation of brine composition data	29
6.2.1 Correlation coefficient and correlation matrix.....	29
6.2.2 Formation water analysis	31
6.2.3 Example: The Slochteren and Delft reservoirs	37
6.3 Thermodynamic calculations	42
6.3.1 Methods	42
6.3.2 Results.....	43
7 Discussion	46
7.1 Scaling	46
7.2 Corrosion.....	48
8 Conclusions	53
References	55

Summary

To understand and predict possible productivity and injectivity problems at the geothermal sites, better knowledge of the mineralogical assemblage of the reservoir rocks and the composition of the formation water is essential. On that background, a comprehensive PERFORM database has been established, which includes geological, geochemical, and geo-mechanical information as well as operational data from sensors at the plants, and the data have been analysed using a range of methods and tools.

Seven key geothermal sites named in the project proposal have shared relevant parts of their data (Thisted, Margretheholm and Sønderborg in Denmark; Groß Schönebeck in Germany; Honselersdijk and Pijnacker Nootdorp in Netherlands; and Schlattigen in Switzerland), and data from additional sites have been obtained from a Dutch database, from the Danish research project GEOTHERM, and from the published literature. Thus, the information represents a variety of geothermal reservoir types and geological settings. To share, present and disseminate data, a PERFORM website has been constructed, managed and maintained by GEUS; refer to <https://www.geothermperform.eu>. In general, the data on the website will be public, but some proprietary data provided by private companies will need to be kept confidential. To resolve this problem, the data of confidential nature will be invisible on the public website.

The collected data have been analysed to check its quality, test analytical tools and elaborate on potential causes for observed productivity and injectivity problems. Application of machine learning techniques to the production data from sensors at the Sønderborg site shows that anomalies in sensor output can be detected automatically. Such variations in the data can reflect many aspects of the operation, but it could be caused by the onset of scaling or corrosion. For time series of data, where gaps exist, machine learning allows estimation of the values for missing datapoints. Such analysis of production data can be used to support the operation of a geothermal well.

Correlation analysis and principal component analysis were applied to identify systematic variations and correlations within the datasets and the tendency for mineral precipitation was determined with thermodynamic calculations. Our interpretations of the results indicate that:

- Calcium carbonate scaling can be largely avoided by maintaining an operational pressure exceeding the bubbling point. The operators of the plants are for most part able to do so.
- The concentrations of Ba and SO_4 in the vast majority of formation waters are at, or close to, equilibrium with barite (BaSO_4) at reservoir conditions but supersaturated at the surface after cooling. Despite this, significant precipitation of barite is only reported at few sites. We interpret that the barite scaling forming here reflect that the produced water is hot and Ca-rich – and that such formation water characteristics are likely to induce barite precipitation. If calculations of saturation states were accurate for a broader range of solution compositions (i.e., in Ca-rich brines), we foresee that the extend of barite formation could be predicted. If formation water composition and temperature can be estimated prior to drilling, risks might even be assessable beforehand.
- For the sites in the database, substantial galvanic corrosion by dissolved Pb or Cu occurs only where these elements coexist with elevated concentrations of chloride in the formation water. Tentatively, the threshold chloride concentration for such corrosion is ~100,000 mg/L.
- Corrosion by oxygen ingress occurs at high rates and may cause the formation of substantial amounts of iron-oxides that can potentially cause clogging of sand screens in injection wells. Therefore, introduction of oxygen into the geothermal water stream should be avoided. Most operators of the plants are for most part able to do so by maintaining an increased operation pressure.
- Data on the corrosion rate from the Sønderborg site, however, indicates that oxygen may well ingress here. In addition, bottom-hole samples at the site contain poorly soluble iron oxides, similar to in nature to the mill scale observed on left over tubing at the surface. This

suggests that the injection problems at the Sønderborg site could stem from inadequately prepared infrastructure, with corrosion possibly promoting the migration of the mill scales.

- Corrosion related to sulphide formation in plants with high sulphate concentrations in the formation water may be a process causing decreased injectivity due to clogging of sand screens with corrosion products. However, the importance of this process is not fully understood and should be subject to future studies.

The results show that operations based on hot, Cl rich formation waters are particularly challenging because of an increased potential for galvanic corrosion. If such waters also contain large concentrations of Ca, the risk of barite scale formation is also increased. Such knowledge could be included during the selection of materials for the infrastructure to minimise corrosion and during the design of the plant to ensure that mitigating measures, such as inhibitors or filters for cation removal, can be timely applied.

1. Introduction

The PERFORM project includes the construction of both a website and a database. The objective is to collect, store and present operational, chemical and physical data from a number of operating geothermal sites within the EU. To our knowledge, no other database containing trans-national information on geothermal data has been established until now. Both the PERFORM website and database focus on uploading existing data, but also new data have been collected and uploaded.

The database and website form the basis of comparing, integrating and evaluating site-specific data, with the objective to:

- Learn from the data collected and understand why operational problems occur at certain geothermal sites/plants.
- Address and resolve major problems, including scaling and corrosion issues.
- Better understand reservoir performance aiming at explaining causes of observed problems.

GEUS, TNO, GFZ and FT have all participated in the effort to establish common knowledge and address major problems.

The main results of work package 1 of the PERFORM project is reported herein. Chapter 2 outlines the process of the data collection – the data types and the origin of the data are described. Chapter 3 gives the structure and information on the created database. Chapter 4 describes and presents the website. Chapter 5 and 6 focus on production data and presents our analyses of the water composition data. Chapter 7 discusses the results. Finally, Chapter 8 presents the conclusions.

2. Data collection

To establish a database available through the PERFORM website, data from approx. 26 sites and another 40 wells were collected. The aim was to include as much information as possible about geological, geochemical, physical and operational aspects for each of the geothermal sites or wells included in the database. However, depending on the specific data source for each entity in the database, the amount of data varies considerably. For a number of key geothermal sites identified initially in the project, detailed information is available while for other geothermal wells, only limited data were available in the literature. The data collection was based on:

- A.** Data from key geothermal sites identified initially in the project
- B.** Additional data from Dutch sites obtained from an in-house TNO database with the permission of operators as well as new data from Dutch reservoirs
- C.** Data collected from a parallel geothermal research project in Denmark (the GEOTHERM project)
- D.** Data collected from the literature

2.1 Data from operators of key geothermal sites

Initially, eight key geothermal sites located across Europe were identified. As part of the project application phase the operators of these sites had agreed to share data in the common knowledge database. These geothermal sites are:

- Thisted, Denmark
- Margretheholm, Denmark
- Sønderborg, Denmark
- Groß Schönebeck, Germany
- Honselersdijk, Netherlands
- Pijnacker Nootdorp, Netherlands
- Schlattigen, Switzerland
- Oberlaa, Austria (no data supplied)

Data were collected using the questionnaire outlined below (Table 2.1). The questionnaire was designed to obtain as much information as possible about basic data, important geological aspects, reservoir parameters, key geochemical data, surface facilities, well design, operational performance and potential injectivity problems.

Table 2.1 Questionnaire on obtaining site-specific data

1. Name of site or site. Basic data	<i>Age of site or site.</i>
	<i>Producing reservoir (depth and lithology)</i>
	<i>Number of wells, well locations</i>
	<i>Distance between production and injection well(s)</i>
	<i>Position (depth) of perforated intervals</i>
	<i>Type and sort of available samples (overall list)</i>
	<i>A list of relevant reports and articles</i>
2. Important geological data	<i>Geological setting and stratigraphy</i>
	<i>Mineralogical composition and chemistry of the reservoir rock</i>
	<i>Depositional environment</i>
	<i>Cores and core descriptions (if available)</i>
	<i>Fracture presence (if any)</i>
	<i>Occurrence of lead/Pb in minerals. Which minerals?</i>
	<i>Extras</i>
3. Information about selected reservoir parameters	<i>Porosity</i>
	<i>Permeability</i>
	<i>Net and gross sand thicknesses</i>
	<i>Formation temperature (of the reservoir zone)</i>
	<i>Formation pressure (of the reservoir zone).</i>
	<i>Flow rate when producing the reservoir, incl. seasonal variations.</i>
	<i>Extras</i>
4. Key geochemical data	<i>Geochemical analyses of the formation water. Chemical composition in mg/L along with sample depths.</i>
	<i>Composition of the dissolved gases in the formation water. Focus on the concentration of CO₂, CH₄, H₂S etc.</i>
	<i>Geochemistry of the injection water.</i>
	<i>Water properties, e.g. pH, density, conductivity, resistivity etc. of both the produced water and the injection water.</i>
	<i>Salt concentration, TDS, mineralization (g/L).</i>
	<i>Initial reservoir temperature. Temperature of the produced water – and the (re-)injected water.</i>
	<i>Initial reservoir pressure (needed for the geochemical modelling).</i>
	<i>In addition: Injection and operating pressures.</i>
	<i>Particles in fluid samples (e.g. in the water produced): What is the particle content, the composition and the particle size?</i>
	<i>Comments on chemical treatment of the injection water (or the reservoir rock). May involve adding chemicals/ inhibitors or removal of chemical reactants.</i>
	<i>Scaling: Composition of precipitating minerals (if scaling is observed)</i>
	<i>Corrosion: Composition of corrosion products (if observed)</i>
	<i>Tables with: Analyses of filtrate samples (e.g. from membrane filters, bag-filters or cartridge filters.</i>
	<i>In case of degassing: Which gasses are observed?</i>
	<i>Analysis of fluid samples originating from flooding experiments.</i>
	<i>Additional data relevant for geochemical modelling (thermo-hydro-chemical processes).</i>
	<i>Geo-mechanical data</i>
	<i>Extras</i>
5. Short description of surface facilities (incl. materials used)	<i>Filters at well head (if cation, particle or similar filters are used)</i>
	<i>Heat exchanger(s)</i>
	<i>Pumps (EPS, heat pumps).</i>
	<i>Materials used in the construction of surface facilities</i>
	<i>Well head</i>
	<i>Comments</i>
	<i>Extras</i>

6. Information about well design (incl. materials used)	<i>Casing and tubing material</i>
	<i>Pipeline material</i>
	<i>Casing depths, vertical wells, deviated wells</i>
	<i>Completion design</i>
	<i>Comment on the use of gravel packs, subsurface filters, screens etc.</i>
	<i>Extras</i>
	<i>Comments</i>
7. Information about operational performance and data monitoring, including on-site measurements	<i>Flow rate as function of time (time series, to be reported in tables)</i>
	<i>Injection rate as function of time (time series)</i>
	<i>Pressure as function of time (time series)</i>
	<i>Temperature as function of time (time series)</i>
	<i>Corrosion rate as function of time (time series)</i>
	<i>Data originating from on-site monitoring of particle size, particle composition, water composition etc.</i>
	<i>Extras/comments</i>
8. Possible mechanisms for injection problems (or reduced injectivity), if observed.	<i>Fines migration.</i>
	<i>Scaling issues (type of scaling, precipitating minerals etc.)</i>
	<i>Inadequate filtering prior to re-injection.</i>
	<i>Precipitation of salts due to cooling.</i>
	<i>Degassing of CO₂, pH increase.</i>
	<i>Bacterial activity (e.g. sulphate-reducing)</i>
	<i>Clogging of pores. Migration of particles.</i>
	<i>Clay swelling (clay clogging).</i>
	<i>Mobilization of particles from the reservoir.</i>
	<i>High mineralization.</i>
	<i>Corrosion issues, leading to clogging/plugging: Galvanic or CO₂ or oxygen corrosion. Also: electrochemical processes, lead/Pb precipitation, H₂S presence etc.</i>
	<i>Gas issues (e.g. degassing, CO₂ that separates out, ingress of O₂)</i>
	<i>Onset of reduced injectivity at a particular injection rate?</i>
	<i>Mitigation strategies (e.g. chemical injection, well work-over etc.)</i>
	<i>Comments on observed re-injection challenges.</i>

2.2 Additional data from Dutch sites

To supplement the information obtained from the eight key geothermal sites, data was collected from 22 Dutch geothermal sites. All active Dutch operators were contacted to request data and obtain their permission to publish new and existing data in the PERFORM database. For the sites where no (complete) dataset was available, geothermal brine samples and/or samples from geothermal wells cuttings (at the TNO core shed) were analysed.

In the Netherlands it is mandatory for operators to provide the advisory group of economic affairs (TNO) and the Dutch state supervision of the mines with certain documents after a new geothermal site is completed. These documents contain data from well tests, water and gas analyses, well design etc. There is a challenge in making these data accessible for the public geothermal community. Firstly, any data provided by the operators remains confidential until five years after delivery and can therefore not be used in other projects without permission from the operator. Also, TNO collects geothermal data in projects jointly with the operators but this data also remains confidential. To use and publish the information available in-house at TNO, operators have to give their permission explicitly.

Therefore, operators were personally contacted by phone and e-mail to ask for their permission to use the data already present in the TNO database. From the 22 geothermal sites, eight gave permission to use their data on the public website (without naming the operator). Thirteen operators could not be reached by phone and did not reply to the e-mail and one operator gave no permission to publicly use the data.

Table 2.2 List of geothermal wells in the Netherlands, their permission for the use of data and the available water, gas and mineralogical data.

Operators	Wells	Available brine data	mineralogy data	Gas data	Missing data	permission
Aardwarmte Vierpolders	BRI-GT-01,02				All	no response
Aardwarmte Vogelaer	PLD-GT-01,02				All	no response
Agriport A7, middenmeer (Ecw)	MDM-GT-01,02,03,04,05,06	Brine analysis well 2	analyse		mineralogy	permission
Ammerlaan	PNA-GT-01,02,05,06	Brine analysis well 1	3x		complete	permission
Californie Lipzig Gielen	CAL-GT-01,02,03	Brine analysis well 1,3			mineralogy	no permission
Duijvestein	PNA-GT-03,04	Brine analysis well 3,4			mineralogy, gas	permission
Floricultura Heemskerk	HEK-GT-01,02	Brine analysis well 1	analyse		mineralogy	permission
Geopower Oudcamp	MLD-GT-01,02				All	no response
Geothermie de Lier	LIR-GT-01,02				mineralogy, brine	no response
Greenbrothers	ZVB-GT-01,02				All	no response
Greenwell Westland	HON-GT-01,02	Brine analysis well 1,2	4x		complete	permission
Haagse aardwarmte Leyweg	HAG-GT-01,02	Brine analysis well 2	2x		complete	no response
Het Grootslag Andijk (Ecw)	ADK-GT-01,02,03,04				All	permission
Hoogweg Aardwarmte	LTG-GT-01,02,03				All	no response
Koekoekspolder (greenhouse g)	KKP-GT-01,02	Brine analysis well 1,2	analyse		mineralogy	no response
Mijnwaterproject	HLN-GT01,02				All	no response
Nature's heat	KHL-GT-01,02				All	permission
Trias Westland	NLW-GT-01,02				All	no response
Van den Bosch 1&2	VDB-GT-01,02	Brine analysis well 2	analyse		mineralogy	no response
Van den Bosch 3&4	VDB-GT-03,04	Brine analysis well 3,4	analyse		mineralogy	no response
Wayland energy	LSL-GT-01,02				All	no response
Wijnen Grubbenvorst	ARC-GT-01,02	Brine analysis			All	permission

2.3 New data acquired for Dutch reservoirs

As a second step, the incomplete datasets of the sites that gave permission for publication were supplemented with new analyses of gas, water and/or mineralogy. Often the water and gas data were already available but mineralogical data was missing. Storage of cuttings or cores from wells drilled in the Dutch subsurface is mandatory and are available for sampling in the TNO core-shed. Cuttings from the targeted wells were sampled and analysed with XRD. Table 2.3 lists all the samples that were collected and from which a selection was analysed.

Table 2.3 List of samples from geothermal wells

Samples	Depth (m)	Samples	Depth (m)
CAL-GT-03		MDM-GT-01	
CAL-03-1	2105	MDM-01-1	2545
CAL-03-2	2000	MDM-01-2	2700
CAL-03-3	2525	MDM-GT-02	
CAL-GT-02		MDM-02-1	2330
CAL-02-1	1420	MDM-02-2	2520
CAL-02-2	1585	MDM-GT_03	
CAL-03-3	1675	MDM-03-1	2540
HEK-GT-02		MDM-03-2	2695
HEK-02-1	2690	MDM-GT-04	
HEK-02-2	2865	MDM-04-1	2440
HEK-02-3	2940	MDM-04-2	2605
HEK-GT-01-S1		VDB-GT-03	
HEK-01-1	2885	VDB-03-1	2066
HEK-01-2	2995	VDB-03-2	2084
KKP-GT-01		VDB-03-3	2014
KKP-01-1	2154	VDB-GT-04	
KKP-01-2	2194	VDB-04-1	1535
KKP-01-3	2232	VDB-04-2	1560
KKP-GT-02			
KKP-02-1	2114		
KKP-02-2	2196		

2.4 Data collected from the Danish GEOTHERM project

Site-specific data from the plants listed below originate primarily from synopsis reports prepared for the Danish GEOTHERM research project. These reports outline operational experiences with a number of geothermal plants located in Sweden, Germany and France (Erlström, 2017; Pastrik and Förster, 2017; Tremosa et al., 2017). The Polish plants are described in e.g. Ura-Binzyk (2019) and Kepinska (2019).

- Lund, Sweden
- Melleray, France
- Châteauroux, St Jean, France
- Neustadt-Glewe, Germany
- Neubrandenburg, Germany
- Waren/Müritz, Germany
- Neuruppin, Germany
- GeneSys Horstberg, Germany
- Pyrzyce, Poland
- Podhole, Poland
- Insheim, Germany
- Achères, France
- Bordeaux Grand Parc, France
- Bordeaux La Bénauge, France
- Bordeaux Mériadeck, France
- Cergy-Pontoise, France
- Mérignac Base Aérienne 106, France
- Pessac Sainge-Formanoir, France

2.5 Supplementary literature data

In addition, data from 40 wells located in the Netherlands, Germany, France etc. have been gathered. These data originate primarily from published scientific articles and literature in general.

3 The PERFORM database

The full version of the PERFORM database contains *both* confidential and released data. This version is used internally among the members of the PERFORM project group. A subset of the data in the database consisting only of released data is publicly available via the PERFORM website. The full database contains information about mainly:

- Geochemical analyses of the formation brine and the injection water (mg/L).
- Analyses of particles (solids) in fluid samples (weight-%).
 - Focus is on content and amounts of solids, along with particle composition and size. Both the formation and injection waters have been considered. The samples stem from downhole, filter bags, surface facilities and well heads.
- Composition of the dissolved gases in the formation water.
- Scaling and corrosion products.
- Description of problems observed when operating the sites (using specific codes).
- Information about surface facilities and well completion designs.
- Geology, depositional environment and mineralogy of the reservoir rocks.
- Reservoir parameters. Porosity, permeability, temperature, gross and net sand thicknesses
- Time series. Variation in flow rates, temp., pressure.
- References (bibliographic).

The public subset of the database can be downloaded from the website:

<http://www.geothermperform.eu/wp-content/uploads/2019/10/backup-20191022.zip>

Apart from a backup file of the database, this zip file also contains a description of code lists, tables and columns and a diagram showing the relation between the tables. To give a visual impression of the database, a Database Diagram is shown in Figure 3.1.

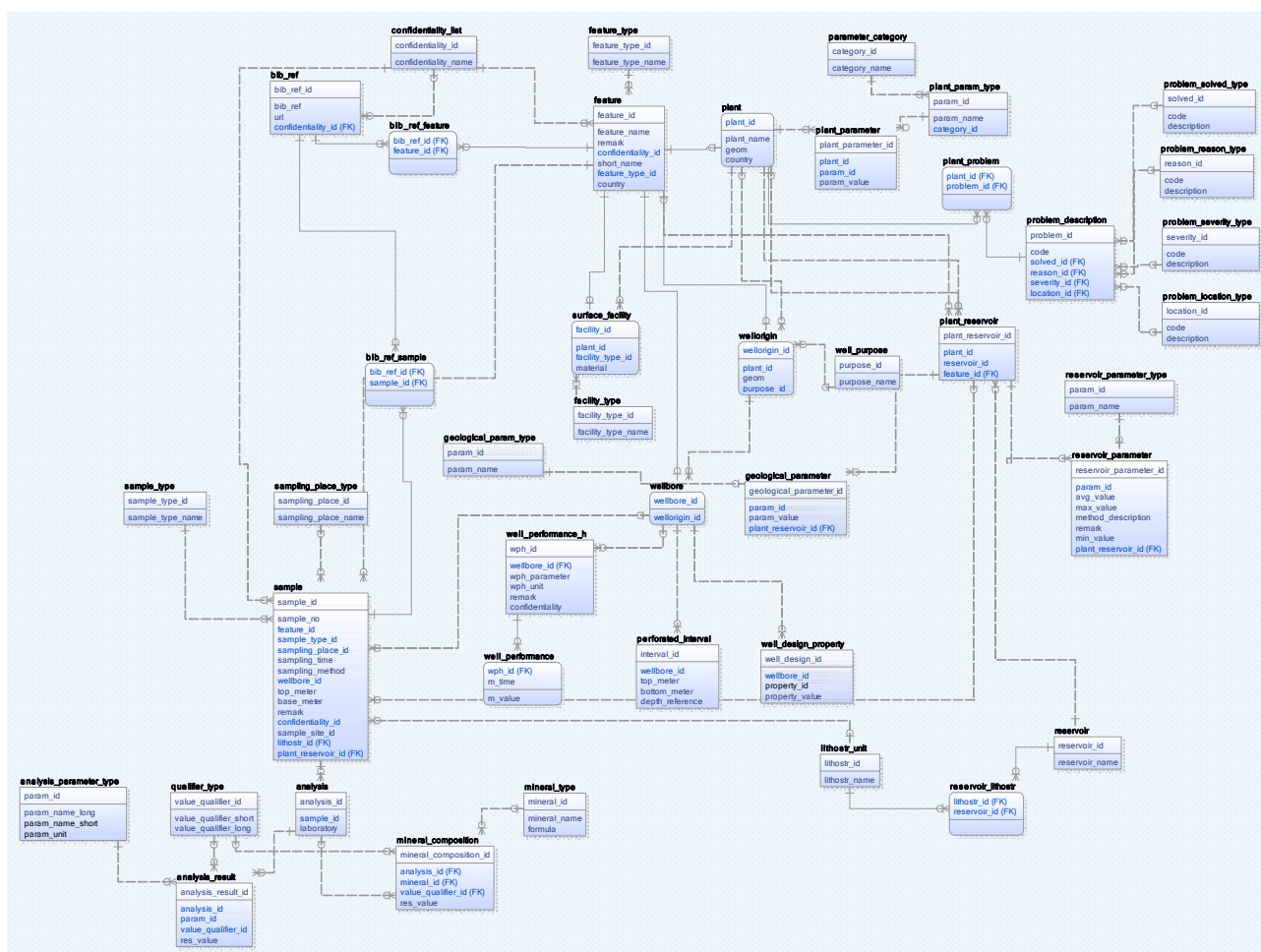


Figure 3.1 Database Diagram for the PERFORM database

The table below lists the number of sample types, feature types and data points in the database (Table 3.1). The numbers shown in the table are expected to increase as the project proceeds.

Table 3.1 Statistics on selected data types in the database

Type of data	Number (October 2019)
Formation water samples	138
Injection water samples	18
XRD analyses	25
Particle analyses	14
Analyses of scaling products	4
Analyses of observed minerals	202
Wellbores	105
Reservoir rock designations	90
Geothermal sites	27
Surface facility indications	26
Datapoints related to time series analyses	1281610
Number of measurements related to a parameter	4933
Sample type, sampling method, well name etc.	199
Reservoir parameter values	167
Bibliographic references	122

4 Website construction

A public PERFORM website was constructed in order to disseminate information gathered in the PERFORM project. Access to the website can be obtained using the link:

<https://www.geothermperform.eu>

The entry to obtaining information from the website is the geothermal site name, either by clicking on the location map shown below or by entering the site name. The website front page is illustrated below.

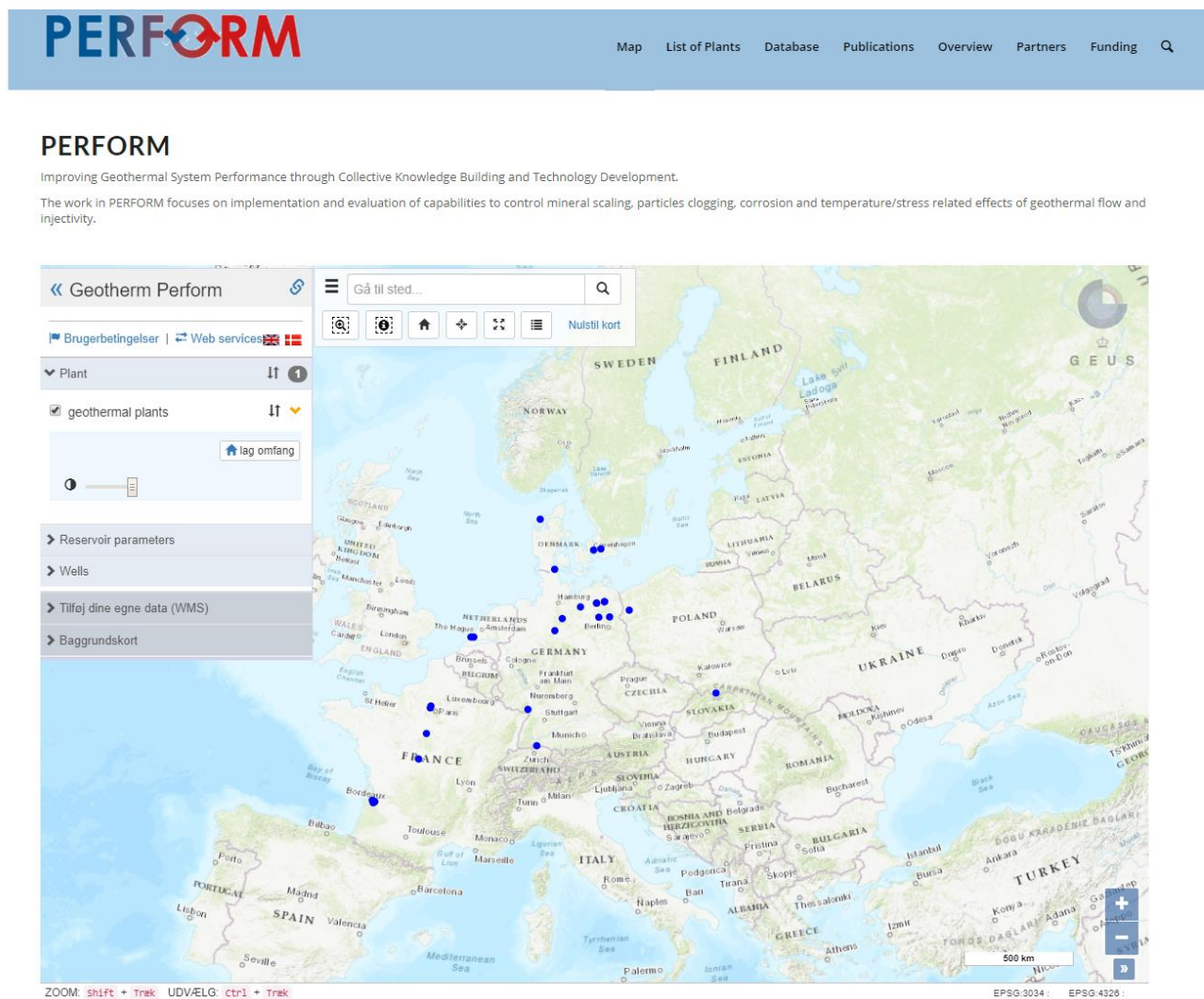


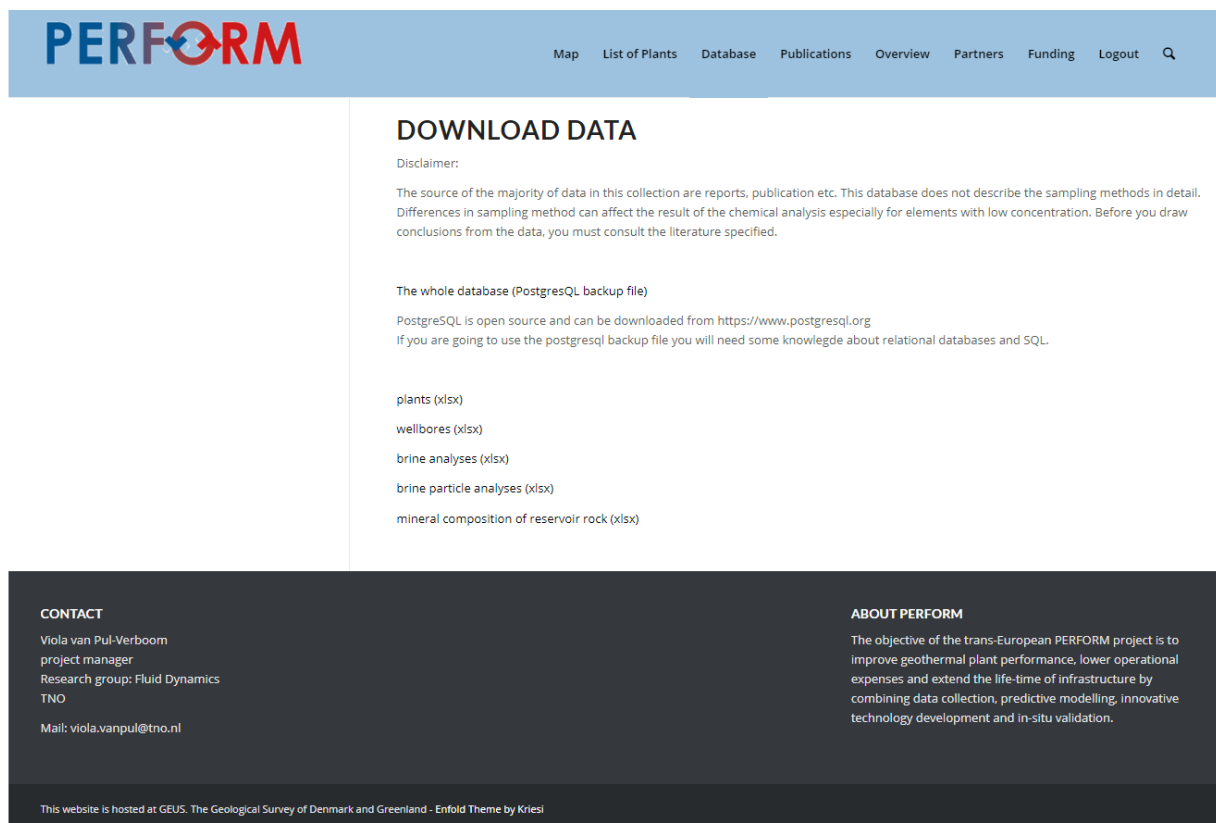
Figure 4.1 The PERFORM website (www.geothermperform.eu)

The PERFORM website includes information about:

- Site locations (a base map is shown on the from page)
- Conceptual sketches of site configurations (only for 6 selected sites)
- Maps with reservoir parameters.
- Link to fact sheets. These sheets include information about the items listed below, if data are available from the operators, research articles, reports etc.:
 - Reservoir rock (sandstone, limestone etc.).
 - Reservoir depth and reservoir temperature.
 - Problems observed in the operating sites.
 - Geological model for the reservoir(s) associated with the operating sites.
 - Well completion design. Only for selected wells drilled at site localities.

From the website, it is possible to download the released data from the database. The database is provided as a zip file containing the following (some data material is password protected):

- A backup file from the PostgreSQL database (SQL statements).
- An ER diagram.
- A dictionary with a description of all tables and columns in the database.
- The content of the code lists.



PERFORM Map List of Plants Database Publications Overview Partners Funding Logout Q

DOWNLOAD DATA

Disclaimer:

The source of the majority of data in this collection are reports, publication etc. This database does not describe the sampling methods in detail. Differences in sampling method can affect the result of the chemical analysis especially for elements with low concentration. Before you draw conclusions from the data, you must consult the literature specified.

The whole database (PostgreSQL backup file)

PostgreSQL is open source and can be downloaded from <https://www.postgresql.org>
If you are going to use the postgresql backup file you will need some knowledge about relational databases and SQL.

plants (xlsx)
wellbores (xlsx)
brine analyses (xlsx)
brine particle analyses (xlsx)
mineral composition of reservoir rock (xlsx)

CONTACT
Viola van Pul-Verboom
project manager
Research group: Fluid Dynamics
TNO
Mail: viola.vanpul@tno.nl

ABOUT PERFORM
The objective of the trans-European PERFORM project is to improve geothermal plant performance, lower operational expenses and extend the life-time of infrastructure by combining data collection, predictive modelling, innovative technology development and in-situ validation.

This website is hosted at GEUS. The Geological Survey of Denmark and Greenland - Enfold Theme by Kriesi

Figure 4.2 The download data page from the website. Accessible via the “Database” link in the menu.

To be able to use the backup file, knowledge about relational databases and SQL is required, which not all users have. For that reason, most data are also provided as Excel files:

- List of sites with name, country and location.
- List of wellbores with name (long/short), purpose and well location.
- List of samples with well or site name, sample type, wellbore name, sampling time, sampling method, interval (top & base), location (country) and source (e.g. bibliographic reference).
- Brine analyses with sample_id, feature name, sample type, sampling time, sampling place, wellbore name, top meter, base meter, confidentiality status, temperature qualifier, temperature, pressure, pH, density, resistivity and concentrations (mg/L) of geochemical elements such as Cl, Br, SO₄ etc.
- Mineral composition of reservoir rock in selected samples with wellbore name, depth, laboratory and amounts of minerals such as Quartz, Plagioclase (albite), Calcite, Mg-Calcite, Ankerite, Siderite, Halite, Sylvite, Pyrite, Hematite, Chlorite etc.

The data model can be downloaded from the website via a link.

5 Analysis of production data

The PERFORM database contains a number of sensor timeseries datasets that relate to the production of four different wells. Such data give an impression of the operational state of the geothermal plant with high temporal resolution and can, potentially, be analysed in real time. Variations in the data can reflect many aspects of the operation, but it could be caused by the onset of processes that in time will be detrimental to the performance of the plant, such as scaling or corrosion. Thus, development of tools for analysis of the data that can be implemented to automatically detect anomalies could allow early detection of indications of plant malfunction. In this section of the report, two case studies are described to show how these datasets, in combination with machine learning techniques, could be used to support the operation of a well. The first case is related to detecting anomalies during production, the second case to predicting missing data as a result of malfunctioning or missing sensors. Out of the four wells for which production data is available, the Sønderborg well covers the longest time period, and has the highest sensor frequency. For these reasons, both cases are demonstrated using the Sønderborg data, but the techniques shown can be transferred to other wells. In the next section, the data set is briefly explored and visualized. In the two following sections, the two case studies are discussed separately.

5.1 Sønderborg production data

The Sønderborg production data set contains values for five sensor measurements: flowrate in Nm^3/h , upstream and downstream pump pressures in bar, and upstream and downstream pump temperatures in $^{\circ}\text{C}$. The timeseries span a period of around 4.5 years with a timestep of 10 minutes. Due to missing data in some of the sensors, the number of datapoints in ranges from 164429 to 234864. Figure 5.1 shows a plot of the entire data set, which clearly shows the seasonal trend of start-up around winter and shutdown around spring.

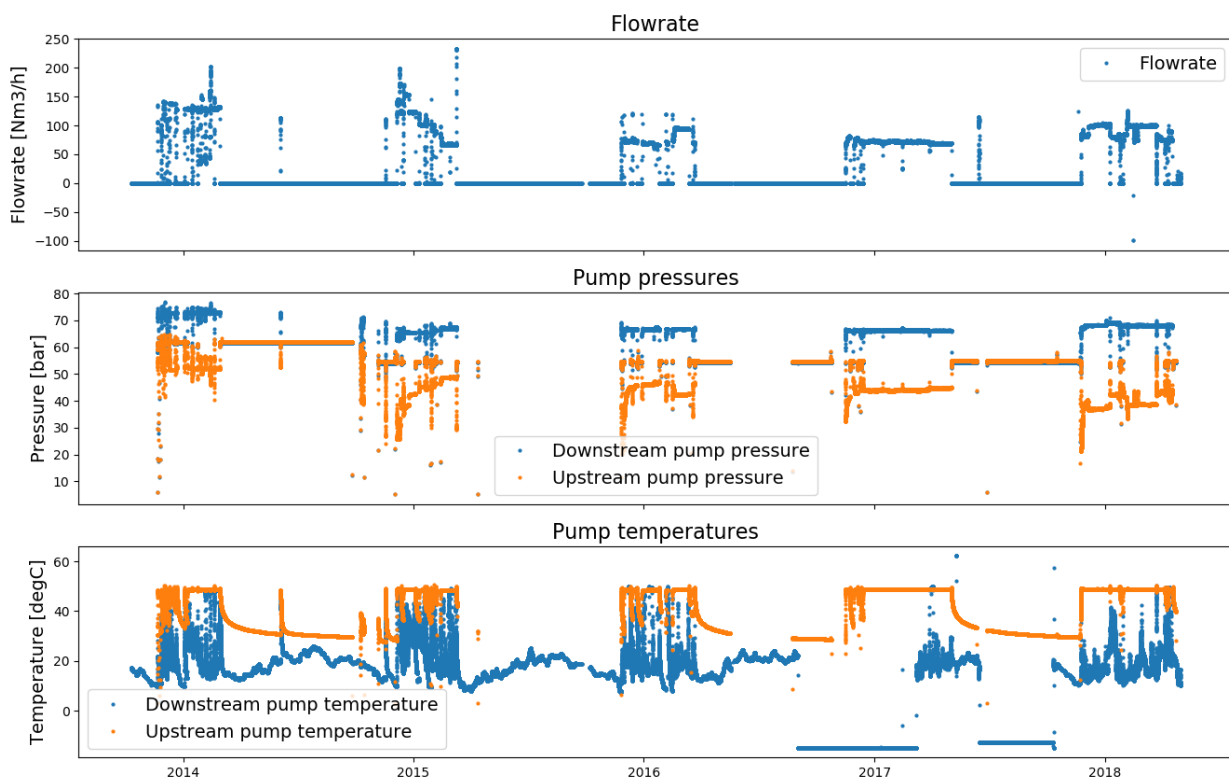


Figure 5.1 Production data of the Sønderborg well

5.2 Anomaly detection

An anomaly is part of a data set that differs significantly from the rest of the data or does not fit within expected behaviour. Anomalies will often occur as extreme-valued data points (outliers), irregular trends, or an increased or decreased frequency of certain values. In the current context of geothermal production data, anomalies will most likely result from sensor failures or problems during production such as corrosion or scaling. It is important to be able to detect these anomalies so that an operator can be warned when production starts to deviate from regular trends, or sensors are malfunctioning. In addition, detecting anomalies in historic data can be useful in order to filter out bad data when only good representative data is required (for example for history matching purposes).

In this case study, machine learning techniques were used to detect anomalous behaviour in the downstream temperature sensor measurements. Figure 5.2 shows a period within the Sønderborg production data in which the downstream temperature sensor suddenly shows large fluctuations occurring without any indication in the other sensors of a reason this could be happening. In the figure, the irregular behaviour has been indicated by the red area, surrounding regular behaviour is indicated by the green region.

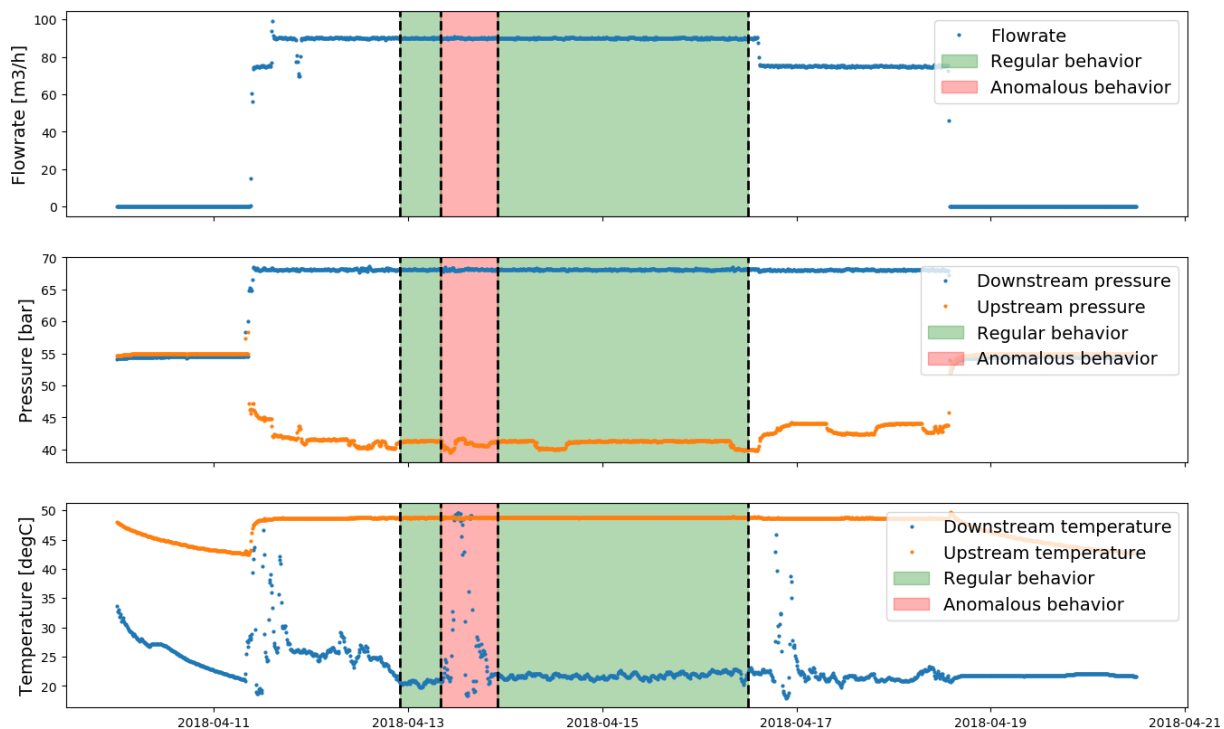


Figure 5.2 A period of the Sønderborg production data showing anomalous behaviour in the downstream temperature

There are many different machine learning techniques that can be used for anomaly detection. In this case study, an "autoencoder" was used. An autoencoder (Baldi, 2012) is a type of artificial neural network consisting of an encoder part, and decoder part (see Figure 5.3). The encoder is used to compress data into a lower-dimensional representation, while the decoder is used to reconstruct the original data from the compressed "encoding". It is possible to tune an autoencoder on data corresponding to regular behaviour such that the difference between original and reconstructed data, the "reconstruction error", is as small as possible. A detailed discussion on the mathematics behind autoencoders and their tuning methods is considered outside the scope of this report, the interested reader is referred to (Baldi, 2012) and (Bishop, 2006).

When the tuned autoencoder is given irregular behaviour to encode and decode, the reconstruction error should be significantly higher than for regular behaviour. By setting a threshold on the reconstruction error above which behaviour should be considered anomalous, a separation can be made between regular and irregular trends in the data. In this way it is possible to express the deviation from regular behaviour of a multi-variate signal in a single number. A considerable change in any of the sensor measurements from the norm would be represented as a significant increase in this number. This simplifies the task of monitoring multidimensional time series data for anomalies.

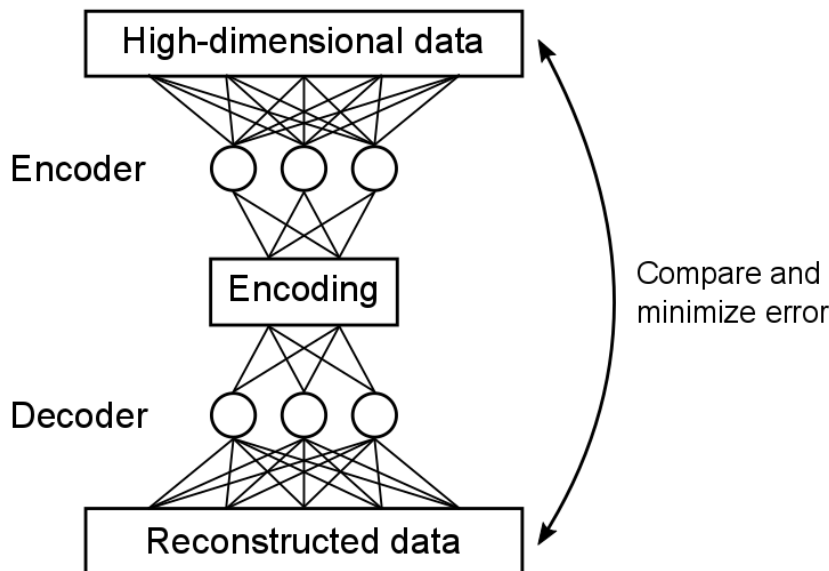


Figure 5.3 Schematic representation of an autoencoder

Using the parts of the production data shown in Figure 5.2 labelled as regular behaviour, an autoencoder was tuned. Figure 5.4 shows the reconstruction error of this autoencoder compared to the original data; the threshold was set as three standard deviations away from the mean of the reconstruction error scored on the regular behaviour only. As can clearly be seen, the error is much larger for the anomalous region than for the regular region, and for the most part well above the threshold. In addition to the clearly anomalous region near the beginning of the signal, there is another brief anomalous period near the end. While there is a slight deviation from the rest of the regular behaviour in this period, it is not very significant, and perhaps should not be flagged as anomalous. This indicates that the current autoencoder might be too sensitive to regular changes, which most likely results from the fact that the current data set of regular behaviour is limited. This was done intentionally to keep the case simple, but the detrimental effects this choice had should be acknowledged here. When moving to a full implementation, it would be advised to tune it to a much larger set of regular behaviour that is representative of the entire production period of interest. Once this implementation is in place, the autoencoder can be used in real-time monitoring: a fixed-size time period of the most recent measurements is continuously encoded and decoded using the tuned autoencoder in order to determine the reconstruction error. If the reconstruction error of newly incoming data rises above the anomaly threshold, the operator can be alarmed. It would also be possible to set a number of thresholds for different severities of anomalies, e.g. one to be used as an early-warning alarm, one for minor anomalies and one for major deviations.

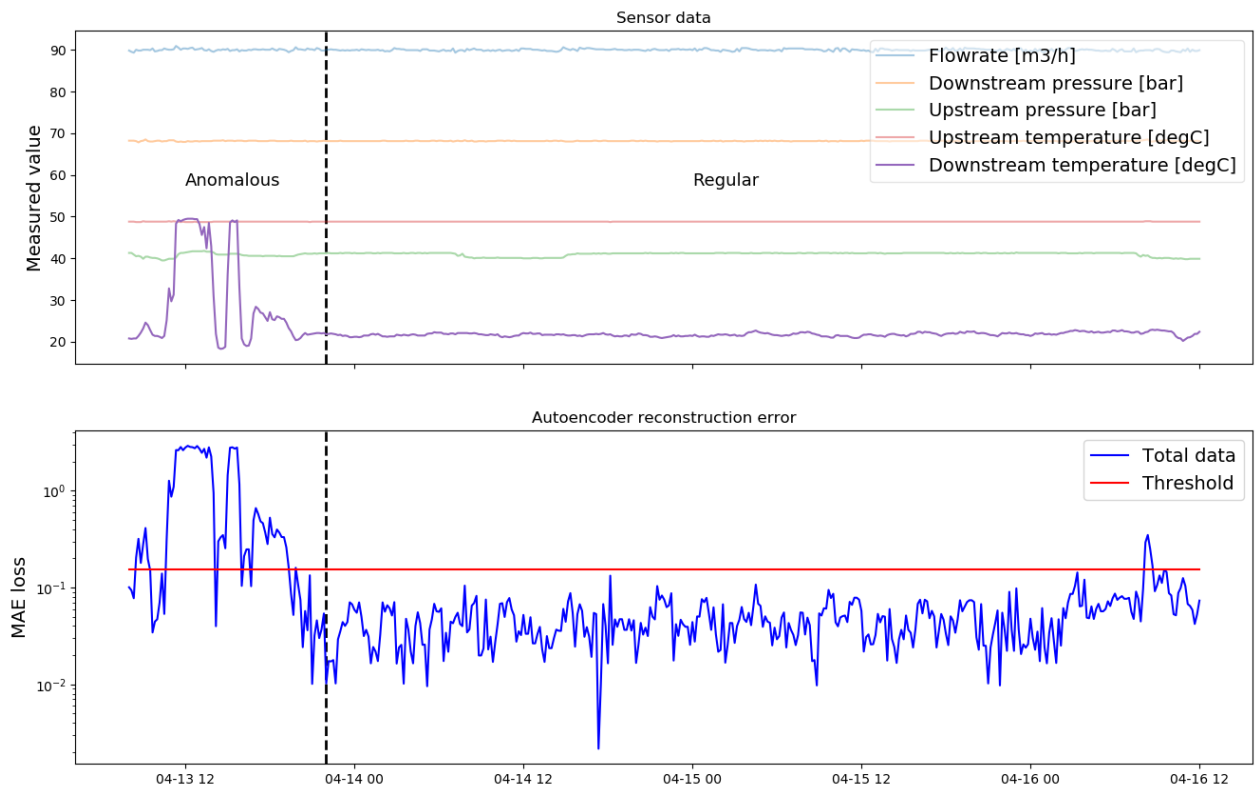


Figure 5.4 Anomalous and regular parts of the production data and their corresponding autoencoder reconstruction error (expressed as mean absolute error MAE)

5.2 Predicting missing data

Certain periods in the Sønderborg production data feature either missing or clearly incorrect measurement values, most likely due to sensor failure or data recording errors. There are many reasons having an estimate of what the sensor should indicate during these periods would be useful. For example, for data analytics / machine learning purposes, history matching, or operational diagnostics. Figure 5.5 shows a part of the production data from the Sønderborg well in which the downstream temperature sensor indicates temperatures of -15 degrees Celsius, comparing this to the rest of the data (Figure 5.1), it can clearly be seen that these are incorrect values. In this case study, machine learning techniques, more specifically Artificial Neural Networks (ANN), were used to predict missing sensor data based on non-missing values of other measurements that were available during this time period.

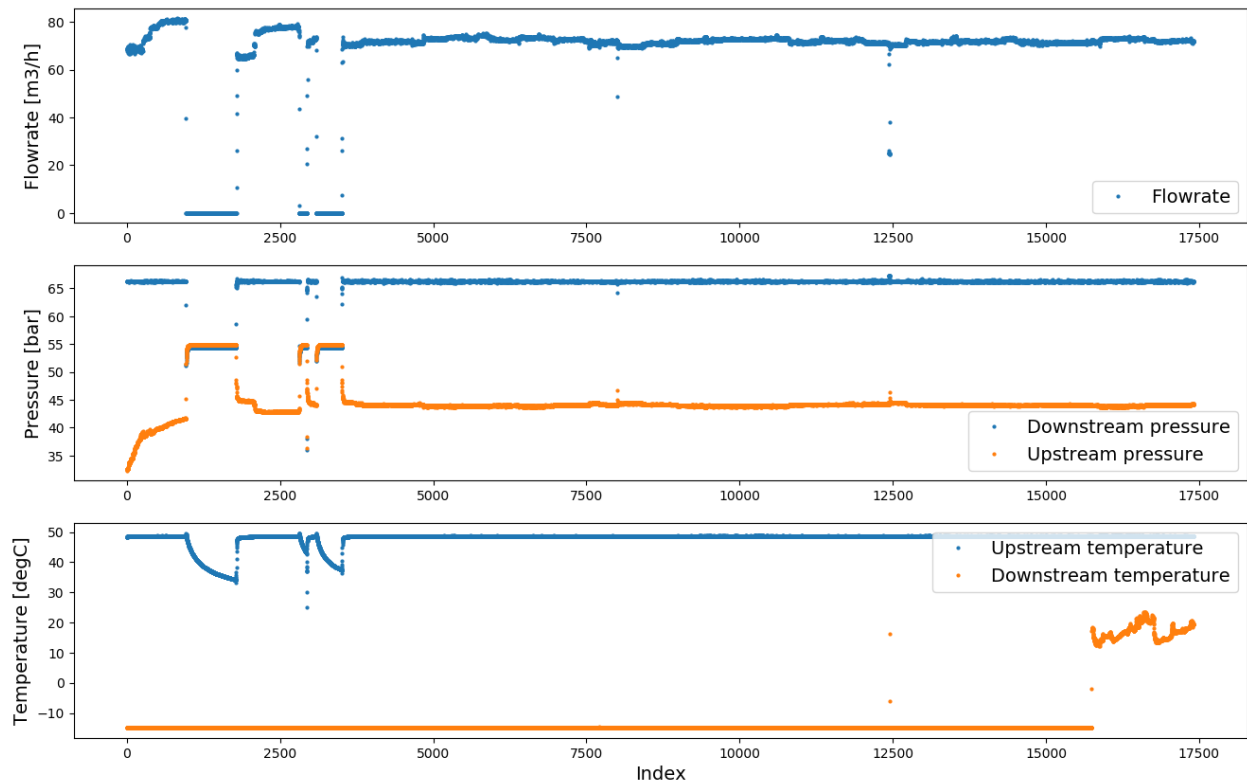


Figure 5.5 A period in the Sønderborg production data containing incorrect downstream temperature sensor data

An artificial neural network is similar to an autoencoder (in fact, an autoencoder is a special type of neural network), but instead of creating an encoding-decoding scheme that reconstructs a given set of data, the network predicts one variable based on other variables. Just as for the autoencoder, the ANN is tuned to a specific data set containing inputs and outputs such that it predicts correctly which output belongs to which inputs. The data used to tune the ANN is shown in Figure 5.6, in this case the input variables are the flowrate, upstream and downstream pump pressures, and upstream pump temperature, while the output is the downstream pump temperature. Again, technical details on artificial neural networks are not considered part of the scope of this report, and the interested reader is referred to (Bishop, 2006).

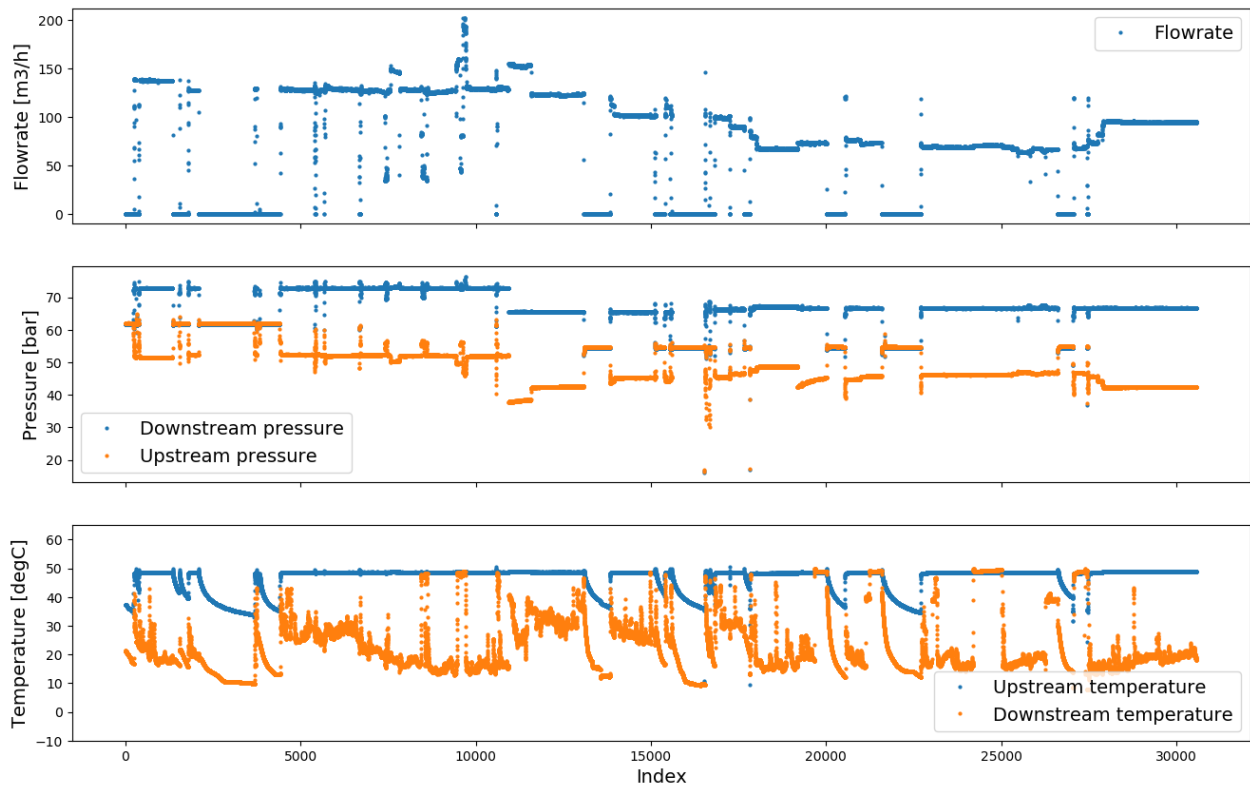


Figure 5.6 Data set used to tune the ANN to predict missing downstream pump temperature values

The predictions made by the tuned ANN are shown on top of the tuning data and test data in Figure 5.7. While the details are not predicted with high accuracy, for most of the time the ANN does manage to model the general trends or behaviour of the system (e.g. when flowrate goes down, temperature goes down). From the bottom plot of Figure 5.7 we can also see that the ANN estimates a temperature for the incorrect period that seems reasonable.

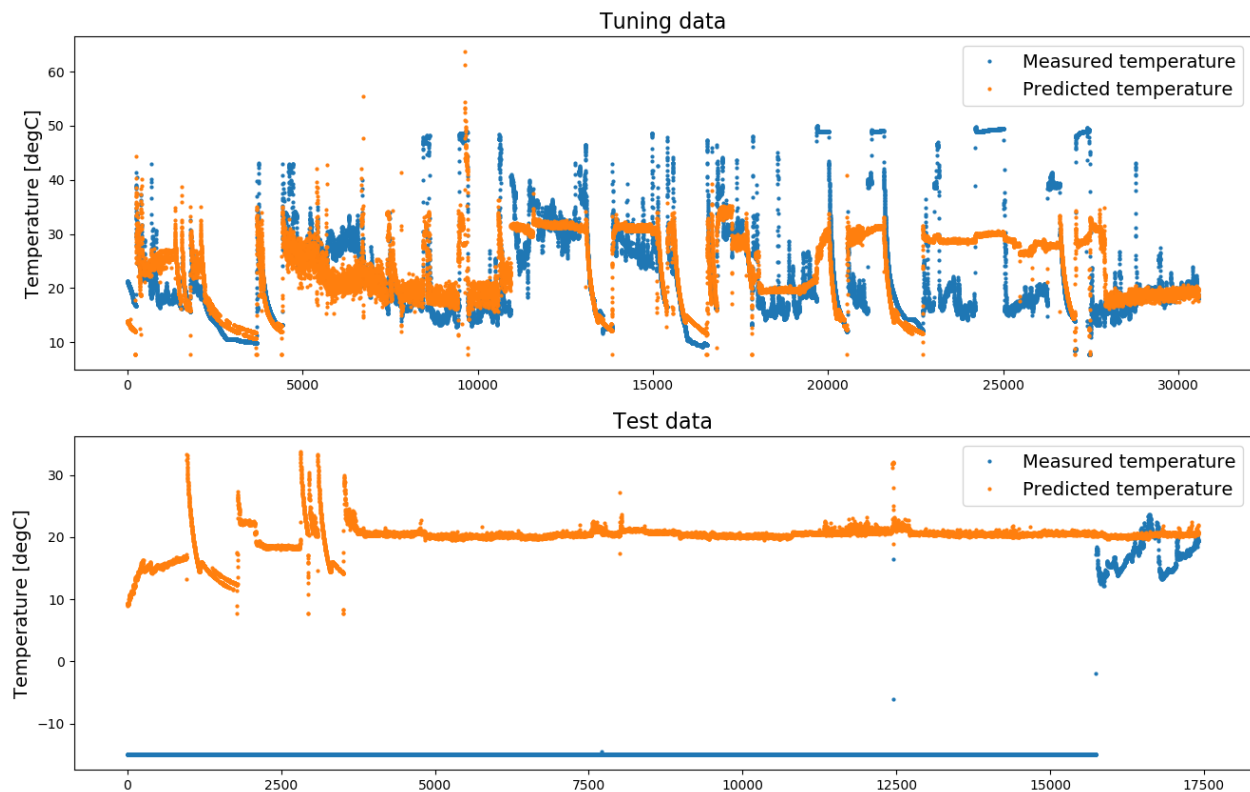


Figure 5.7 Downstream temperature predictions made by the ANN

While the results from the initial ANN were not completely unsatisfactory, it was believed that it could be improved. By looking at the data, it was established that the variables used as inputs were not the only variables affecting the downstream temperature. As can be seen from Figure 5.1 during the summer periods, pressures and flowrates are constant and the upstream temperature is slowly decreasing, but the downstream temperature is varying quite a lot. As these variations seem to follow a seasonal trend, it is likely due to ambient temperature fluctuations. This inspired the idea of using weather data as an additional input to the ANN to see whether it would improve the accuracy of the ANN.

A script was written that downloaded hourly weather data from the Sønderborg area from the website of the Danish Meteorological Institute (<https://www.dmi.dk/>) and aligned it with the rest of the data. The resulting data set is plotted in Figure 5.8, as can be seen the variation in downstream temperature clearly follow the ambient temperature trends.

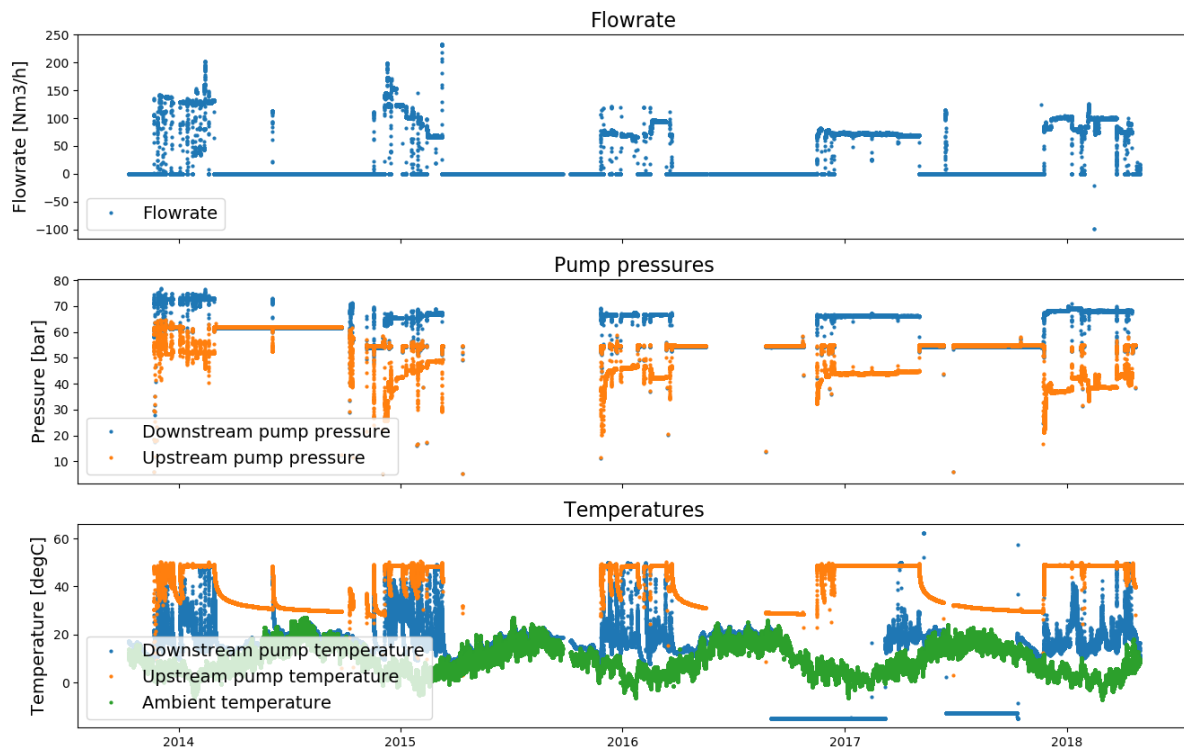


Figure 5.8 Søndersborg production data including weather data retrieved from the Danish Meteorological Institute

A new neural network was tuned including the ambient temperature as an input variable, all other specifications were kept the same as before. The predictions made by this network are compared to measured data as well as the previous results in Figure 5.9. The new ANN shows similar behaviour as the previous one, although the general trends are followed more accurately this time, especially near the end of the tuning data set. When it comes to filling in the incorrect values, the new ANN shows a similar baseline of temperature, but fluctuates much more. While this makes the data look more natural, whether it is also more accurate to the real values cannot be determined.

This brief case shows that using artificial neural networks makes it possible to estimate the value of missing sensor data based on historic sensor measurements and current values of other measurements. This would be useful in general when a sensor is malfunctioning, while a general estimate of its value is still desired. In addition, it could also be used as an anomaly detection measure when sensors are working properly: if the real measurement values start to deviate significantly from the neural network estimates, it could indicate irregular operation.

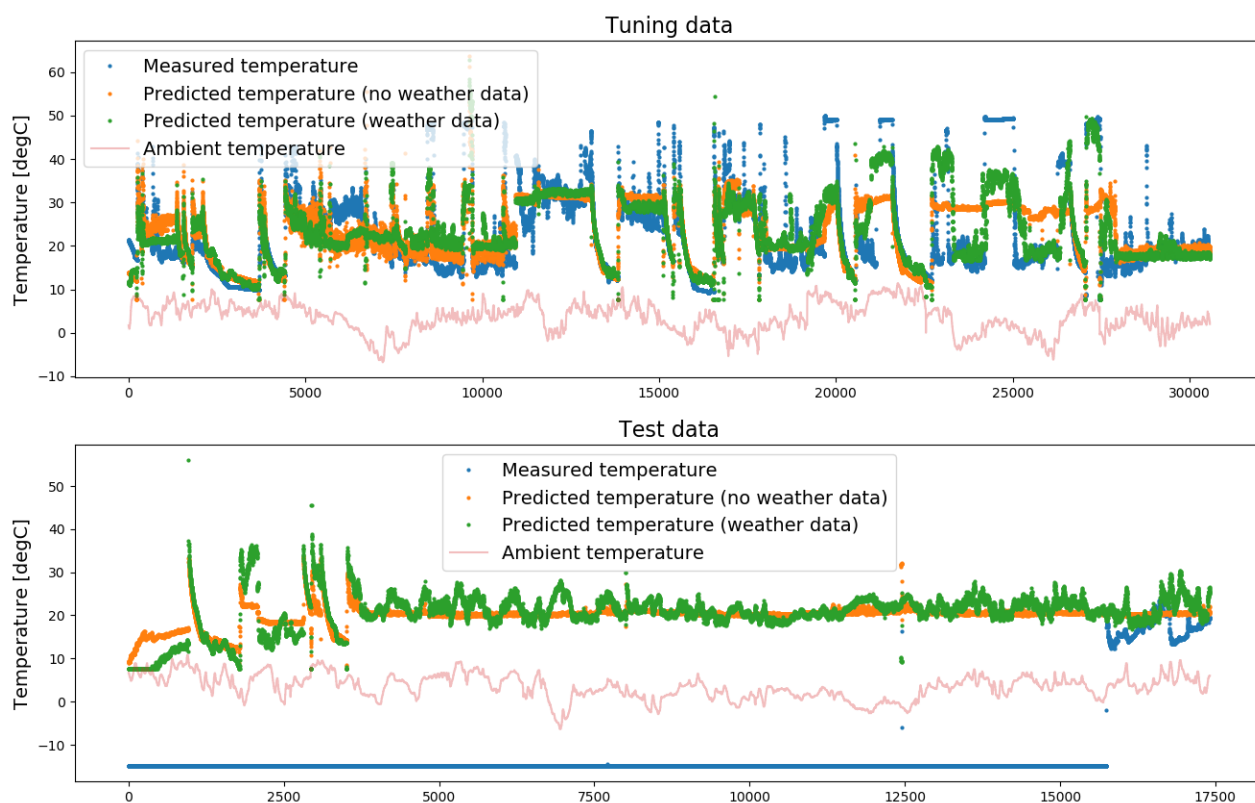


Figure 5.9 Downstream temperature predictions made by the ANN also tuned on ambient temperature data

6 Analysis of data on water composition

One great advantage of collecting a large data set from many sites for the chemical composition of waters is that tools intended for analysis of larger datasets can be applied to get new insights and identify common chemical trends across sites and country boundaries. Here, we have used principal component analysis and correlation analysis to identify systematic variations and correlations within the datasets. In addition, we have probed the tendency for mineral precipitation as scales via thermodynamic calculations.

6.1 Principal Component Analysis

The database contains a large amount of chemical brine/water analyses from several sites located in different countries and in different geological settings. To categorize the water compositions and to identify potential trends in the data material, a Principal Component Analysis (PCA) was carried out.

The PCA method reduces the axes that are needed to describe the variation in a dataset. Fewer diagrams are thus needed to show compositional differences between the samples. The database contains 247 samples of geothermal water from 92 different sites (plants, boreholes, springs, reservoirs, etc.). PCA does not accept missing data, meaning that only a few parameters can be used in the PCA, if all sites are to be included in the analysis. Consequently, only the concentrations of Cl^- , SO_4^{2-} , Na, Ca, Mg, K were used to include the majority of sites in the initial analysis. The parameters were normalized prior to the PCA, and thus weighted equally.

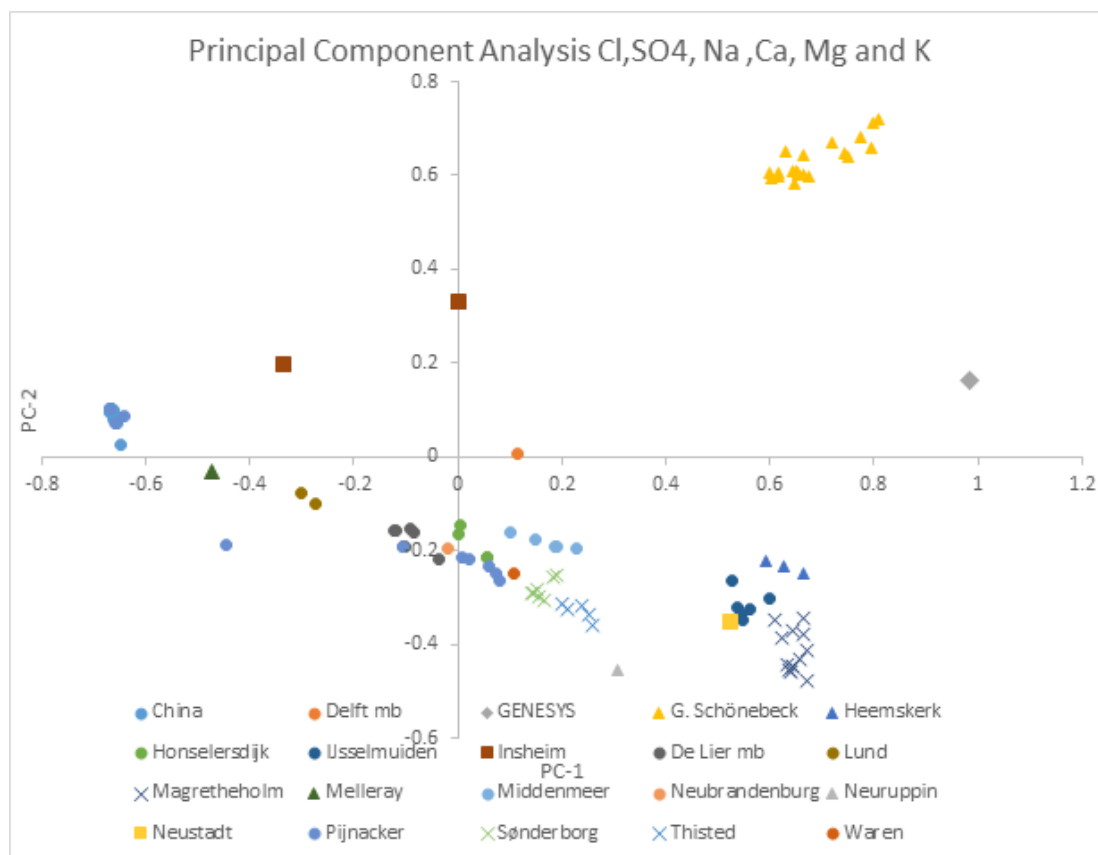


Figure 6.1 PCA of brine composition using six parameters. Score plot for the PC-1 and PC-2 axes.

The diagram in Figure 6.1 shows a score plot for the principal component axes PC-1 and PC-2. This diagram covers 89% of the variation in the dataset. The samples that are seen to the left originates from geothermal sites in Poland and China. These are low salinity brine samples. The salinity generally increases to the right along the PC-1 axis. Interestingly, the variation described by PC-1 and PC-2 can be broadly reduced to three endmembers and mixtures thereof for practically all sites: Endmember 1, with composition of the low salinity brines; Endmember 2, with a composition given by the Groß Schönebeck waters; and Endmember 3 given by the compositions at the Heemskerk, Margrethholm, Neustadt and IJsselmuiden sites. For several of the sites, their data points are aligned along lines connecting Endmember 1 and Endmember 2 or 3. This is most pronounced for Gross Schönebeck, but also occurs to some extent for samples from Pijnacker Nootdorp and Middenmeer. Given our interpretation of the PCA data, this suggests that some of the waters sampled at Groß Schönebeck may in particular be affected by dilution by a low salinity component or perhaps by evaporation (either prior or during sampling or during sample treatment). Apart from these variations, datasets on composition from a given site generally plot tightly with similar scores for the two PCs, suggesting that the chemical compositions measured at different points in time in general are similar.

Another use of the diagram is to compare sites and their described problems – if any. As an example, four out of the five operating sites with a high score for PC-1 (Figure 6.1) have reported formation of substantial amounts of metallic Cu or Pb (Gross Schönebeck, Margrethholm, IJsselmuiden, and Neustadt). In contrast, at Insheim the occurrence of metallic Pb is not reported, although the concentration of Pb in the brine is twice as high as at the Margrethholm plant (1.6 mg/L at Insheim, 0.8 mg/L at Margrethholm). This indicates that not only Cu and Pb but also the general brine composition, i.e. high salinity, significantly affect corrosion with ions of Cu or Pb as oxidants.

Conversely, the Thisted site has been running since 1984 without problems, whereas the Sønderborg site is currently not operating. Yet, the data points of Thisted and Sønderborg are close to each other in the diagram (Figure 6.1). The lack of match between the general brine composition and the degree of problems reported for these two sites, suggests that the Sønderborg site performance may be controlled by processes that are not (only) related to the brine composition.

To put the above analysis into perspective, another PCA was performed with 13 parameters: pH, HCO_3^- , Cl^- , SO_4^{2-} , Na, Ca, Mg, Sr, K, Fe, Mn, Ba and Pb. This reduces the dataset to 107 samples from nine different sites. Due to the altered data space (Figure 6.2), the PCA- axes have changed direction compared to the diagram above but the pattern and grouping among the sites are approximately the same. Therefore, the addition of more parameters does not change the conclusions above.

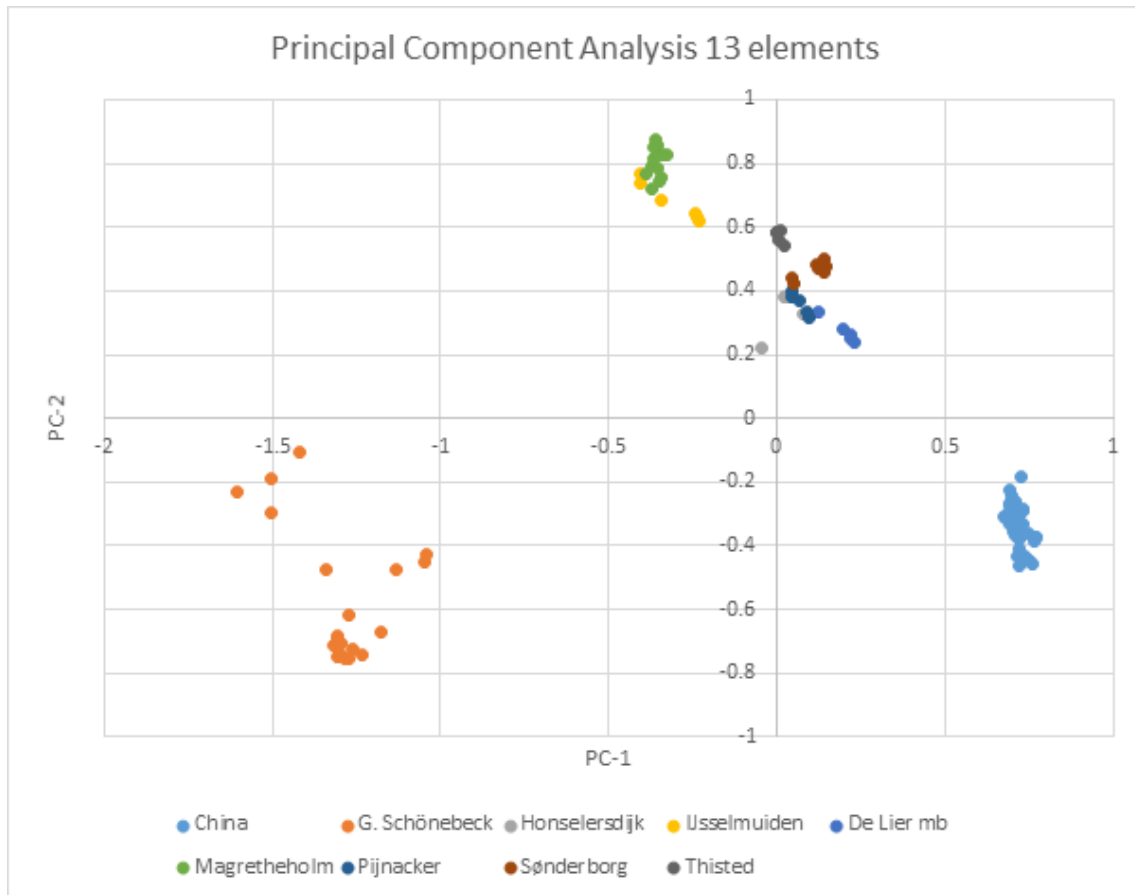


Figure 6.2 PCA on brine chemistry using a dataset with 13 parameters. Score plot for the PC-1 and PC-2 axes.

6.2 Correlation of brine composition data

Correlation between two variables can give an indication of how much their trends are aligned. In this case study, correlations between species found in the formation water of wells in the database were determined in order to investigate whether common or well-specific relationships could be found. The next subsection will give a short explanation of the correlation coefficient, and how to interpret a correlation matrix. In the following section, the results of the analysis will be given and discussed.

6.2.1 Correlation coefficient and correlation matrix

Two variables are said to be correlated if one of them increases, the other (linearly) will increase or decrease with it (or vice-versa). Correlation can be expressed numerically through a correlation coefficient, of which many different definitions exist. The standard correlation coefficient used in most correlation analysis is Pearson's coefficient (Bruce & Bruce, 2017), and has therefore also been used here. This correlation coefficient definition results in a number ranging from +1 to -1, where values above 0 indicate positive correlations, and values below 0 indicate negative correlations. A value at or around 0 means there is little to no correlations between variables.

The correlation coefficient can be visually interpreted by plotting the two variables against each other. The closer the points on this plot lie on a single straight line, the closer they are correlated, this is illustrated in Figure 6.3. Note that the correlation measure is independent of the slope of the line. For

more details on the correlation coefficient, its properties, and how to compute it, the reader is referred to Freedman et al. (2007) and Bruce & Bruce (2017).

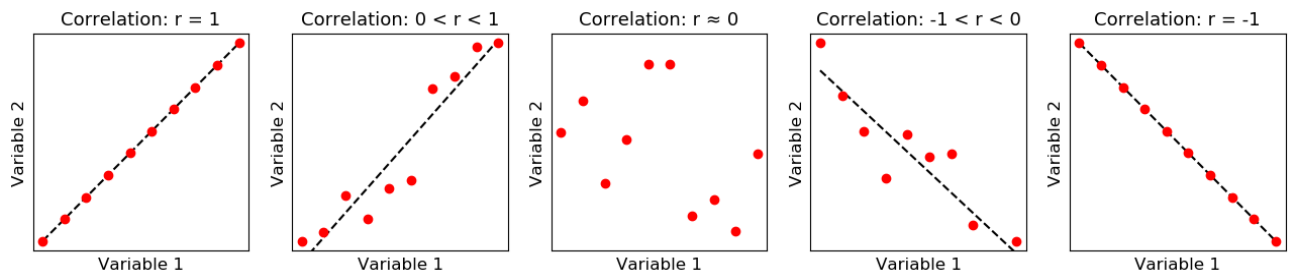


Figure 6.3 Visual representation of the correlation coefficient

In this case study, many variable combinations will be analysed at the same time, making it difficult and cumbersome to plot and interpret each resulting correlation graph individually. For this reason, only the values of the correlation coefficients will be reported. In addition, as all correlations investigated are combinations of the same set of variables, they can be graphically represented in a correlation matrix plot. For an example correlation matrix, see Figure 6.4. The correlation matrix is a square grid whose x- and y-axis are equal and correspond to the variables under investigation. Every element in the grid (matrix) is a combination of two variables and is coloured to reflect the value of the correlation coefficient between these two variables; green for positive values and red for negative values. The correlation between variables X and Y is found by determining the element in the matrix where row X intersects column Y – and comparing its colour with the colour bar right of the matrix. As the correlation between a variable and itself is always 1, all elements on the diagonal of the correlation matrix will always have a value of 1 and be dark green in colour. Furthermore, the correlation between X and Y is the same as the correlation between Y and X, thus the correlation matrix is symmetric across the diagonal.

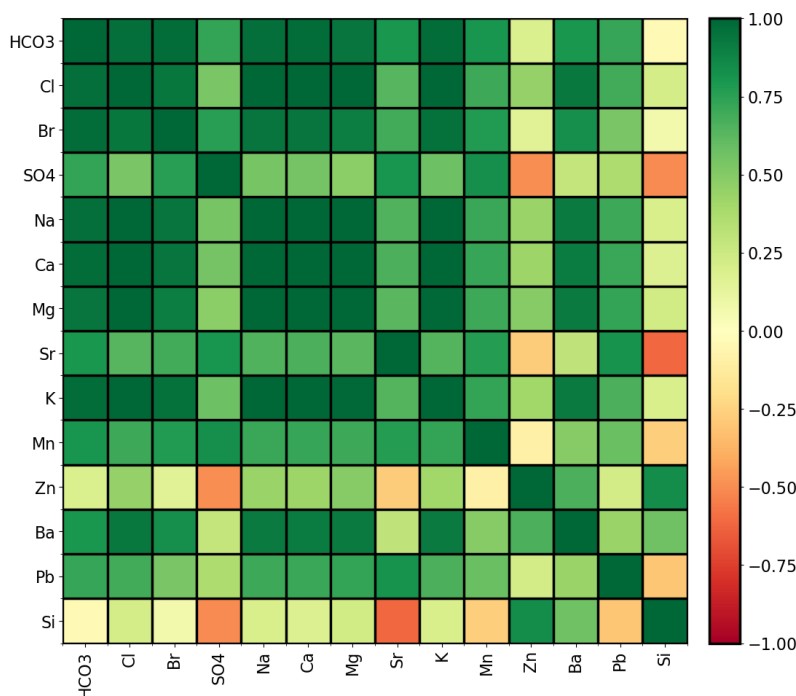


Figure 6.4 Example of a correlation matrix plot

At what value a correlation coefficient can be considered significant is always difficult to define, and often depends on the field of application. In the following sections an absolute value of 0.7 or higher will be considered as significant. It should also be noted that the correlation coefficient can only be used to express *linear* relationships. Due to the complexity and variety of non-linear relationships they have not been taken into account in this analysis.

6.2.2 Formation water analysis

The formation water composition data set contains around 138 measurements for more than 30 different wells. The first correlation analysis looks at behaviour of individual wells and how they compared against each other. In order to ensure the calculated correlation coefficients are significant, only wells with more than 2 measurements were taken into account; this left the Gross Schönebeck, Margrethholm, Sønderborg Fjernvarme, and Thisted Varmeforsyning wells for the analysis.

Figure 6.5 shows the correlation matrices of the four wells with the most measurements, the numbers in parentheses behind each species indicate the number of data points for that species. Note that the Thisted well has at most four measurements for any given species, thus the correlation values reported for this well are much less robust than the other wells and should be interpreted with care. As can be seen, the Gross Schönebeck and Thisted Varmeforsyning wells show mostly positive or no correlation, while the Margrethholm and Sønderborg Fjernvarme show considerably more varied correlations, both strongly positive, strongly negative, and no correlation. There are several species combinations that stand out, for example Na-Cl and Ca-Cl for the Gross Schönebeck and Thisted Varmeforsyning, Na-HCO₃ for Margrethholm, and Br-HCO₃, Na-SO₄ and Mg-Ca for Sønderborg Fjernvarme. The overall positive correlations for many of the components of the Gross Schönebeck and Thisted Varmeforsyning datasets could indicate that the samples from the sites have at some point undergone dilution with a low salinity solution or having experienced evaporation.

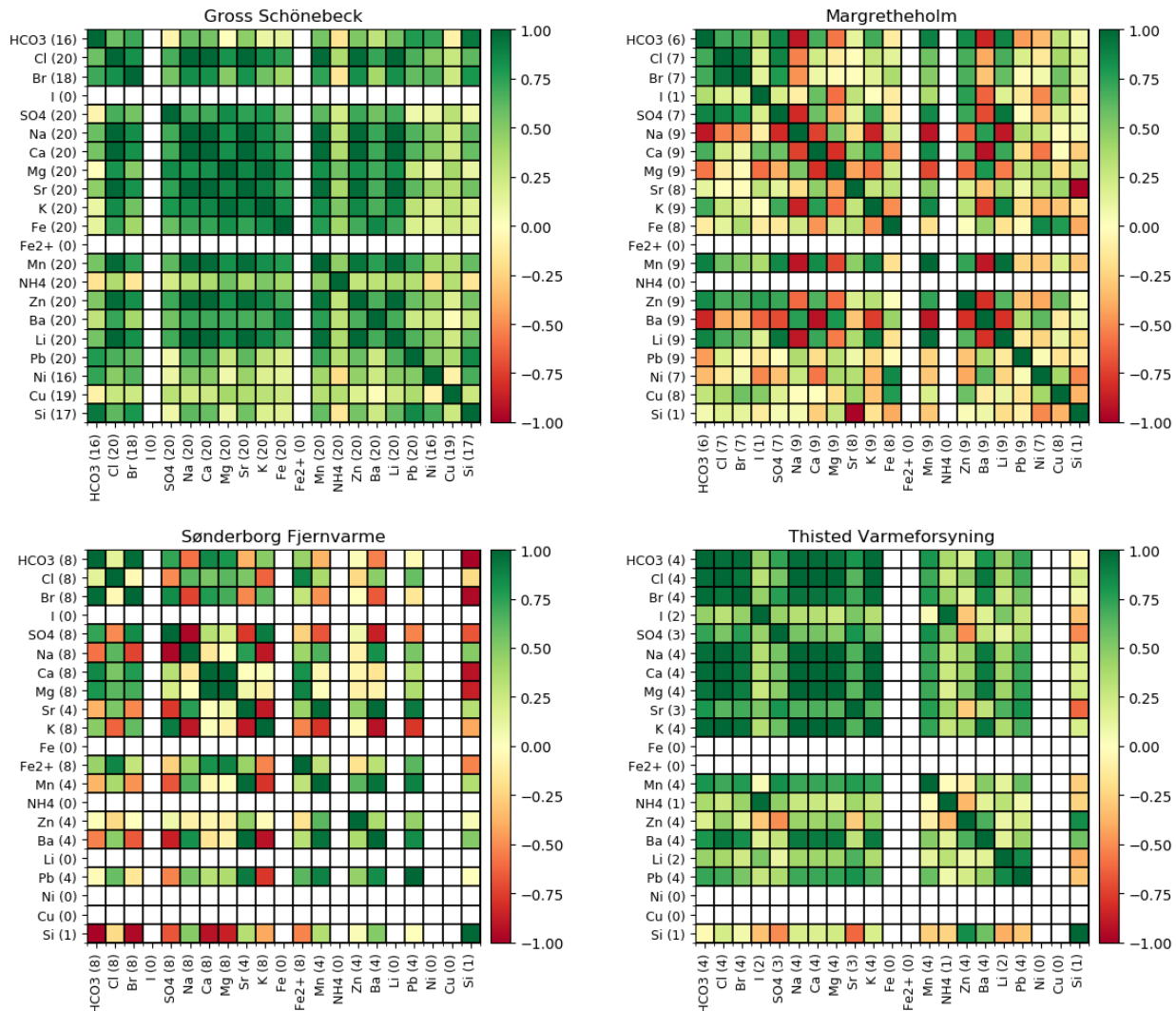


Figure 6.5 Correlation matrices of the four wells with the most measurements. The numbers in parentheses indicate the number of data points for that species

In order to investigate the similarity between these four wells, their correlations have been compared by taking the absolute difference between the coefficient values. The result of this is a matrix of matrices shown in Figure 6.6, in which the colours of the elements in the matrices correspond to the difference in correlation value. The maximum difference value is 2, indicating that the combination of species has completely opposite correlation value for each of the wells (i.e. positive 1 for one well, negative 1 for the other). The lowest value of the difference is zero, corresponding to equal correlation values of a species combination. In the matrices of Figure 6.6, only species for which measurements were available for all four wells were taken into account. Matrices containing more blue elements indicate a closer similarity between wells when it comes to correlations of the species found in their formation water. As can be seen from the figure, the Gross Schönebeck and Thisted Varmeforsyning show the closest similarity.

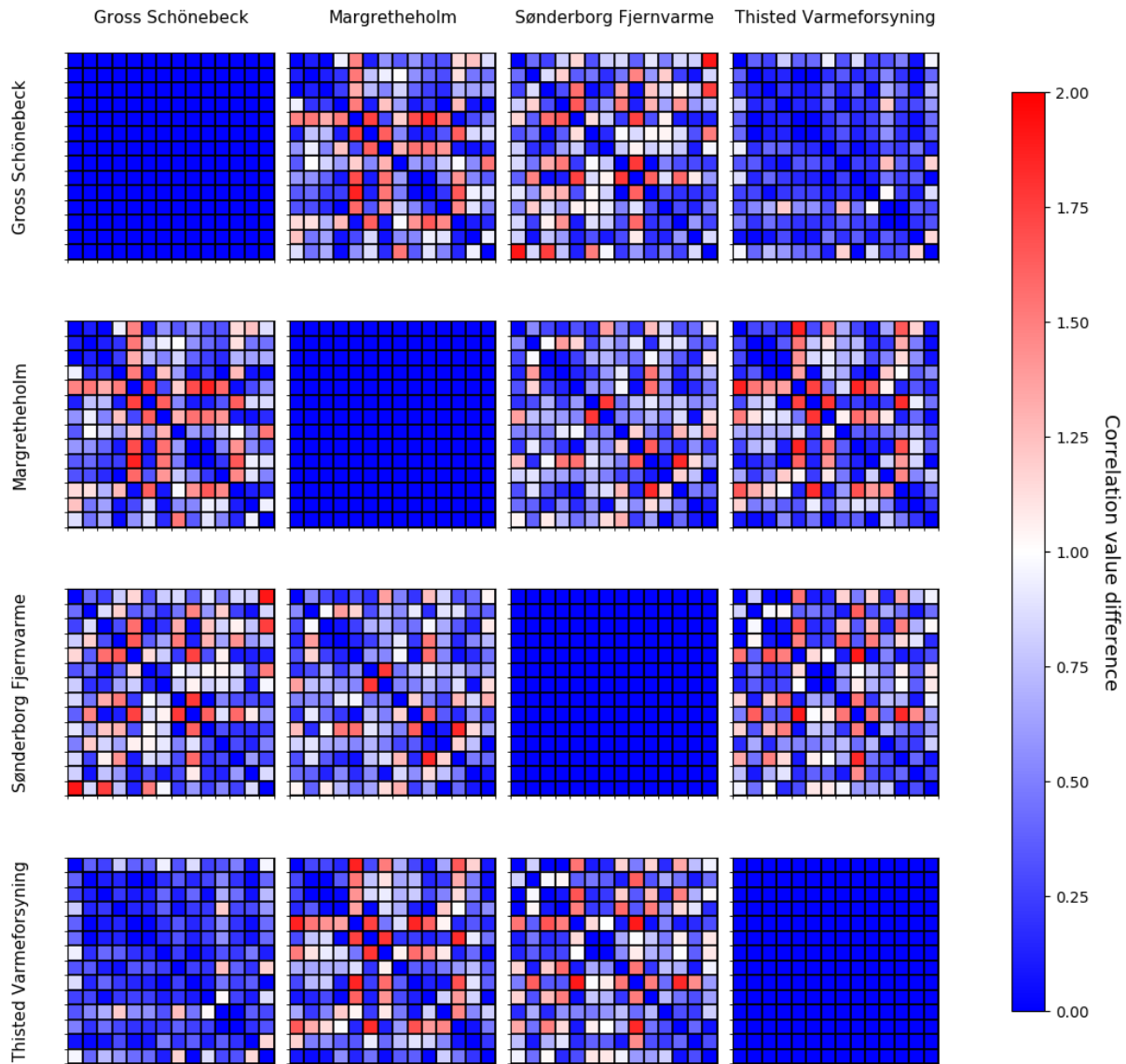


Figure 6.6 Correlation coefficient value difference matrices comparing the four wells with most measurements against each other

In the prior analysis, four individual wells have been analysed and compared to each other. In the following section, the entire formation data set will be investigated, and the four wells will be compared to it in order to determine how the general trends compare against the individual trends.

Figure 6.7 shows the correlation matrix constructed using all samples found in the formation water data set, as can be seen, the correlation values are generally less pronounced, and no significant negative correlations are present. Some of the species combinations that stand out as having a strong correlation are: Na-Cl, Ca-Cl, Mn-Ca, and K-Ca. In addition, one of the strongest negative correlations is observed between Ba and SO₄. This would be expected if the solubility of barite governs both of their concentrations.

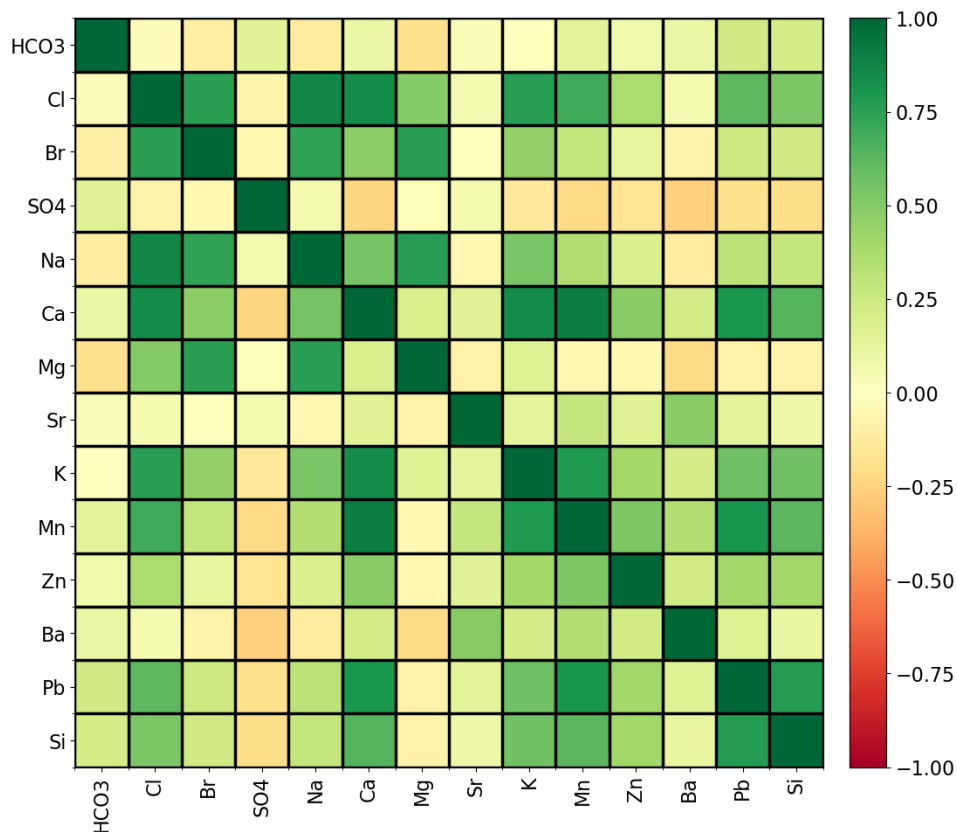


Figure 6.7 Correlation matrix determined using all samples in the formation water data set

To see how the four individual well correlations shown in Figure 6.5 compare against the overall correlations shown in Figure 6.7, four difference matrices can be constructed, similar to those in Figure 6.6. These difference matrices are shown in Figure 6.8. The figure shows that out of the four wells, the Groß Schönebeck well most similar to the total correlation. As the Thisted well was found to be similar to the Schönebeck well, it is unsurprising that it is also close to the overall correlation matrix. It should be mentioned that the Schönebeck well contributes 28 of the 138 samples to the data set, so its similarity to the entire data sets slightly biased. The other two wells also show some close similarities but contain a number of large differences. For example, the Margretheholm well differs largely in its correlation between Na and Cl, as well as K and Na, while the Sønderborg well differs in correlation between K and Cl, Si and Ca and Mn and K.

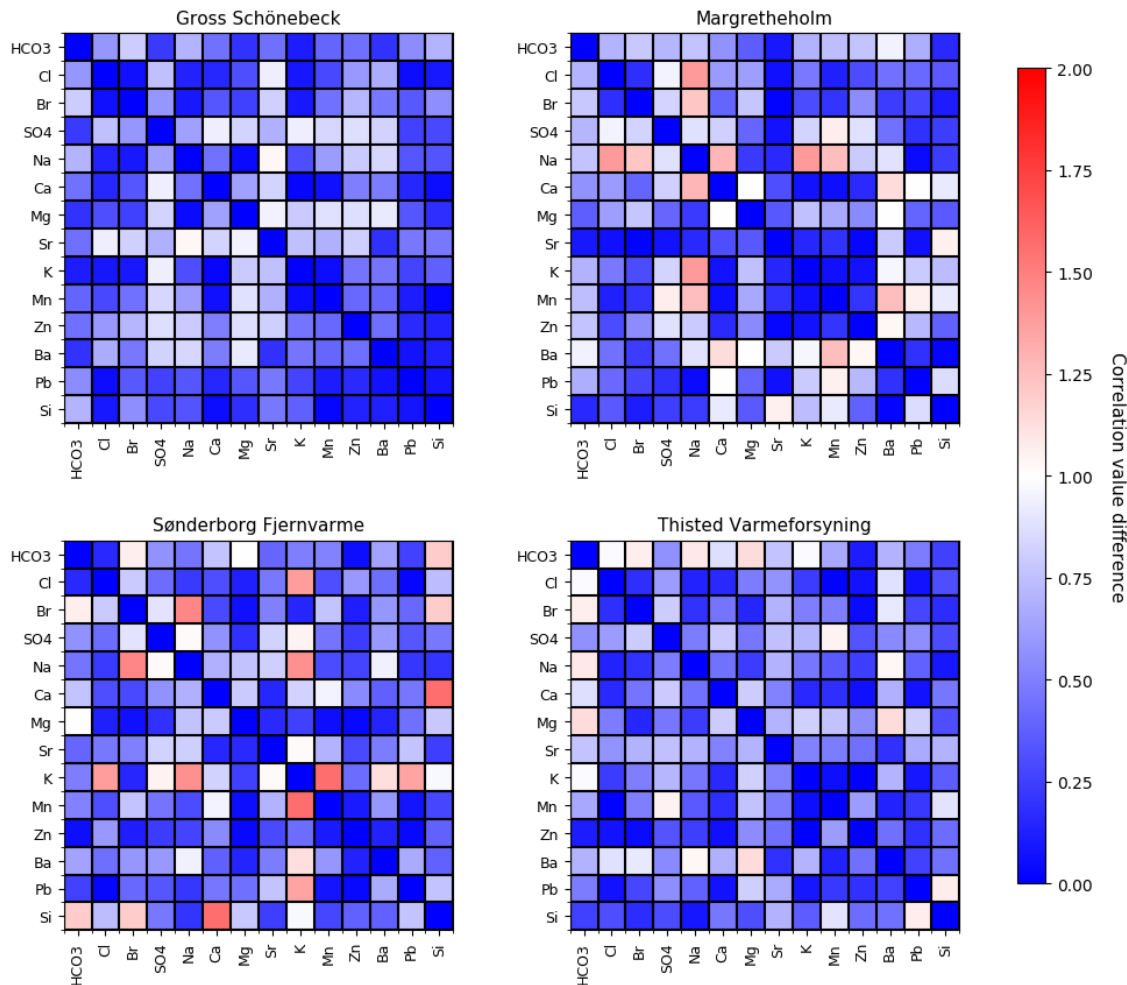


Figure 6.8 Correlation coefficient value difference matrices comparing the four wells against the total correlation matrix

While the previous analysis can be used to find correlations that are specific to each of the wells, it is also interesting to look at which correlations show significant similarities or differences between all four wells and the total. This is done in two ways: by looking at how many of the wells have correlation values that are either close to or different from the overall data set correlations (i.e. look at the difference values of the matrices in Figure 6.8, and for each species combination see how many of the four wells have a corresponding value that is either below 0.2 (similar) or above 0.5 (dissimilar)), and by looking at species combinations that have significant positive or negative correlations in common with the overall correlation matrix. The results of this analysis are shown in Figure 6.9, note that since no significant negative correlations were found for the overall correlation matrix of Figure 6.7 all elements in the bottom right matrix have a value of zero (there can't be any shared negative correlations if one matrix has no negative correlations). From this analysis we can create three groupings in the species combinations:

- Species combinations that often share similar correlations between individual wells and the overall trend, these are the dark-coloured elements in the top and bottom left matrices of Figure 6.9 and include: Br-Cl, Pb-Cl, Pb-Zn, K-Ca, Mn-Ca, and Mn-K. These combinations could be used to indicate general trends that are shared between most individual wells.
- Species combinations that show large differences in correlation between individual wells and the overall trend, these correspond to dark-coloured elements in the top right matrix and

include: Br-HCO₃, SO₄-Br, Ca-SO₄, K-SO₄, Mg-Ca, and Ba-Na. These combinations could be used to characterize individual wells, as they show large variance.

- Species combinations that show neither close similarities, nor large differences. These are the largest group of species combinations. From a characterization perspective, these combinations would be of lesser interest.

One interesting thing to note is that for the species combinations that share similar correlations between the wells, there are at most three wells with similar correlations values, and always one that stands out from the rest. For 4 out of the 6 of these species combinations it is the Sønderborg well that does not share the correlation with the overall correlation matrix. This seems to indicate that the Sønderborg is the most different from the other wells in this analysis.

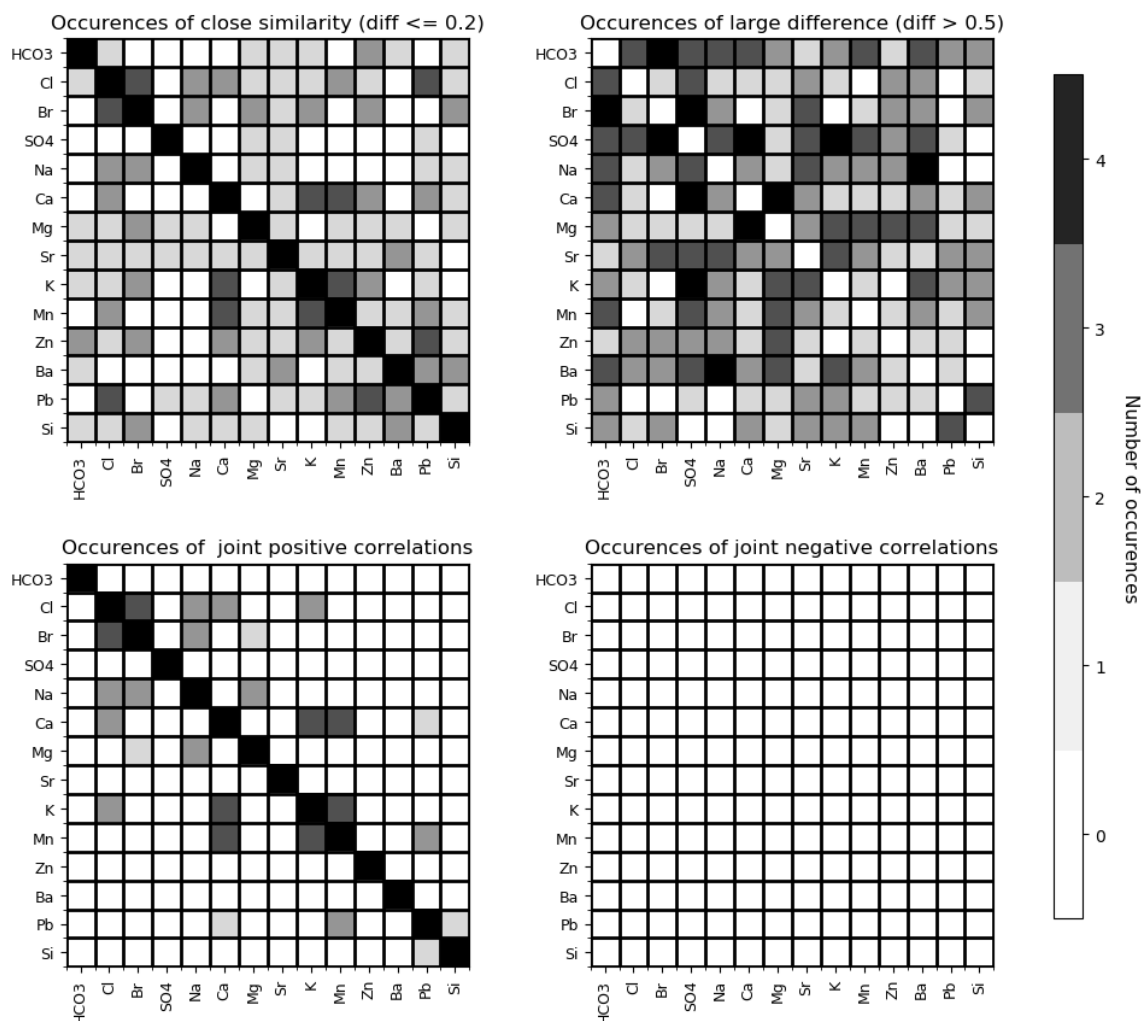


Figure 6.9 Similarity occurrence matrices. Colours indicate how many of the four individual wells show similarity with the overall data set

In this section correlation analysis was performed on the formation water composition data from the PERFORM database. Analyses were performed for the four wells that had the most amount of measurements available. Using the resulting correlation coefficient values, the four wells were compared to each other, as well as the correlations found in the total dataset. From the comparison between the four wells, it was found that the Schönebeck and Thisted well data are quite similar.

However, due to their lack of significant negative correlations, the suspicion arose that some of the samples might have been diluted, skewing the results. No other clear explanation for their similarity could be identified.

In the second part of the analysis, the four individual wells were compared to the correlation coefficients of the entire data set. From this a number of species-pairs were identified that either showed large similarity between the individual wells and the overall trend, or large variations. These pairs could in the future be used to characterize the trends of an individual well with respect to general trends. For instance, it might be of interest to further investigate a well whose correlation between potassium and calcium (a pair that normally shows similar correlation values across wells) deviates significantly from the general trends.

The correlation analysis of the four individual wells indicates that the correlation result of the Groß Schönebeck data as well as the Thisted data is very similar to the total correlation result. The total correlation relates all samples in the entire dataset. Contrary, the Margrethholm data differ largely in the correlation between Na and Cl, as well as K and Na, whereas the Sønderborg data differ in the correlation between K and Cl, Si and Ca and Mn and K.

6.2.3 Example: The Slochteren and Delft reservoirs

Calcite scaling is a commonly observed issue in geothermal installations. The occurrence of calcite scaling is controlled by pressure and temperature changes, but also by several geological and geochemical parameters such as mineralogy of the reservoir, CO₂ content, amount of dissolved Ca and HCO₃ in the brine. The amount of dissolved CO₂ in the reservoir appears to greatly influence the risk of scaling, especially when CO₂ degasses. The gas, water and mineralogical data in the database was analysed in order to constrain the relations between these parameters.

CO₂ concentrations

There are two reservoirs from which the majority of the geothermal sites in the Netherlands produce. These are the Slochteren reservoir (part of the upper Rotliegend) and the Delft sandstone reservoir (part of the Schieland group). The Slochteren Formation consists of pink/red sandstones and conglomerates deposited in an aeolian- or marine environment. The Delft sandstone member is a fluvial deposit consisting of sandstone layers with clay intervals (Van Adrichem Boogaert & Kouwe, 1993). Figure 6.12 shows the stratigraphy of the Dutch subsurface with red circles around the interval of the two reservoirs. In figure 6.10 and 6.11 the CO₂ concentrations that were measured in gas analyses at the sites are plotted. The figures show that even though the data is scattered the average CO₂ concentration measured in the Slochteren reservoir is significantly higher at 22% in comparison to 6% in the Delft sandstone reservoir. This implies that the CO₂ concentrations can be correlated to the different reservoirs.

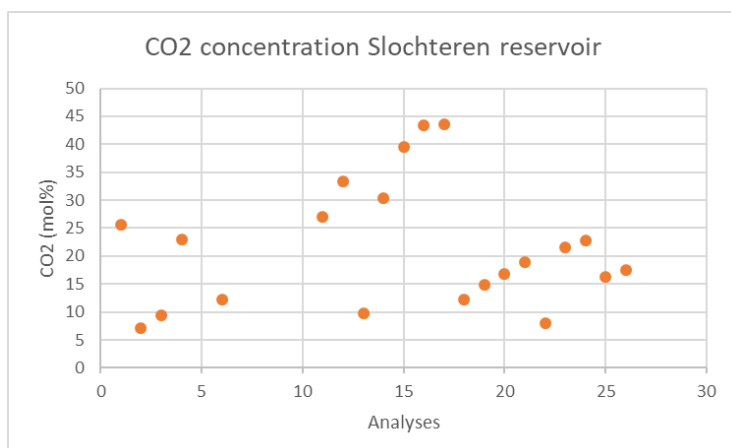


Figure 6.10 CO₂ concentration in mole % measured in wells that produce from the Slochteren reservoir

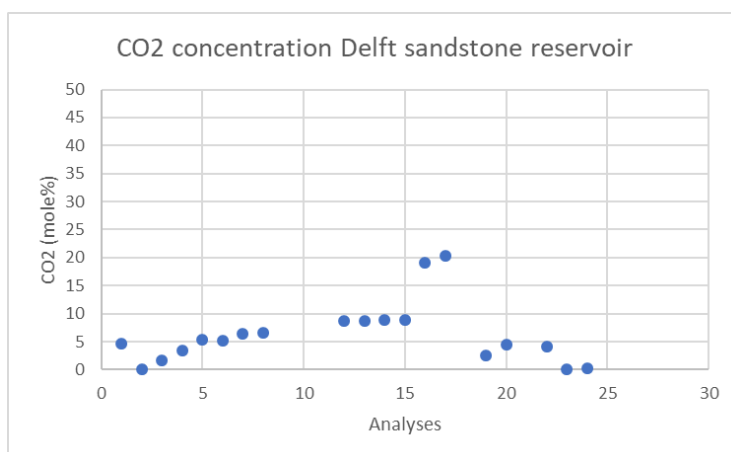


Figure 6.11 CO₂ concentration in mole % measured in wells that produce from the Delft sandstone reservoir

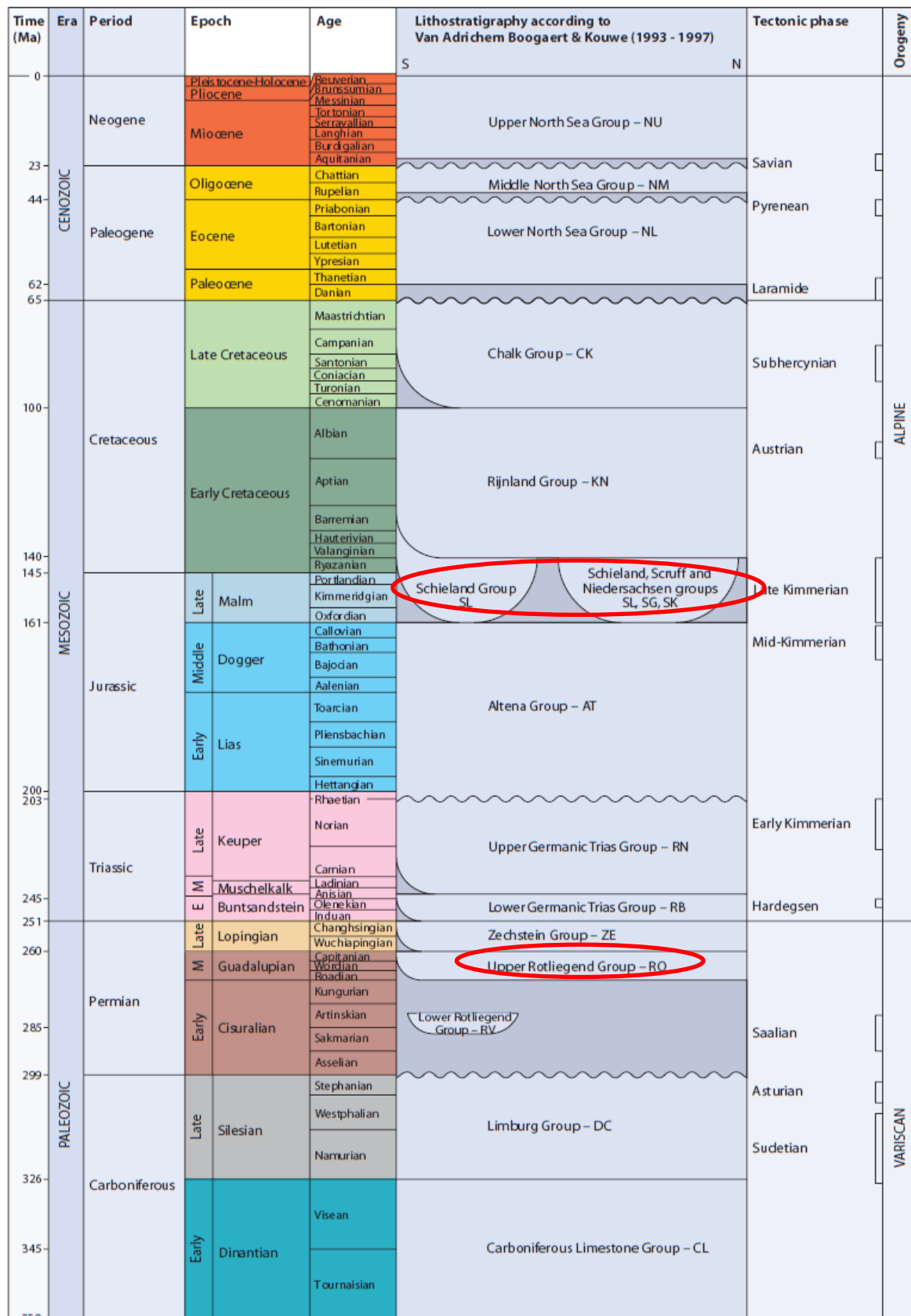


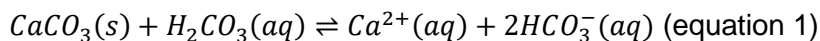
Figure 6.12 Lithostratigraphic column with red circles indicating the location of the Slochteren formation and the Delft sandstone member. (Van Adrichem Boogaert & Kouwe, 1993)

Correlation analysis

In order to characterize similarities between the two reservoirs and to observe overall trends a correlation analysis was carried out, using the same approach as used in Section 6.2. This was done for two cases. First a correlation analysis was done using the formation water compositions. The approach in the first analysis was to not target specific elements but to use the whole dataset. In this way any bias is avoided, and possible unknown relations can be identified.

In the second analysis a different approach was executed. The parameters that are known to relate to scaling processes (not only for calcite scaling but also barite scaling) were used in the analysis. Calcium, bicarbonate, partial pressure of CO₂ and CO₂ mol% and Calcite weight % were included to investigate the process of calcite scaling. Magnesium is included because it can replace calcium to create dolomite. Strontium and barium are included to investigate possible processes related to barite scaling.

The results are presented in Figures 6.13 and 6.14. With respect to the formation water analysis for Slochteren, there is a strong correlation between sodium/potassium and sodium/barium. Another correlation is between magnesium/strontium and calcium. In the Delft reservoir analysis these relations are not observed. There is a negative correlation for both reservoirs between sulphate and calcium. There are clearly stronger correlations for the Slochteren in comparison with the Delft data. In the second analysis in Figure 6.14 a similar overall pattern can be discerned of stronger correlations in the Slochteren data with respect to the Delft data. The negative correlation between Ca and HCO₃ was not expected since these are the elements that form calcite minerals and therefore should be positively correlated (see equation 1).



Another issue for the correlation analysis of the second case, especially for the delft is the low number of datapoints, which makes the results hard to interpret (see X's in figure 6.9).

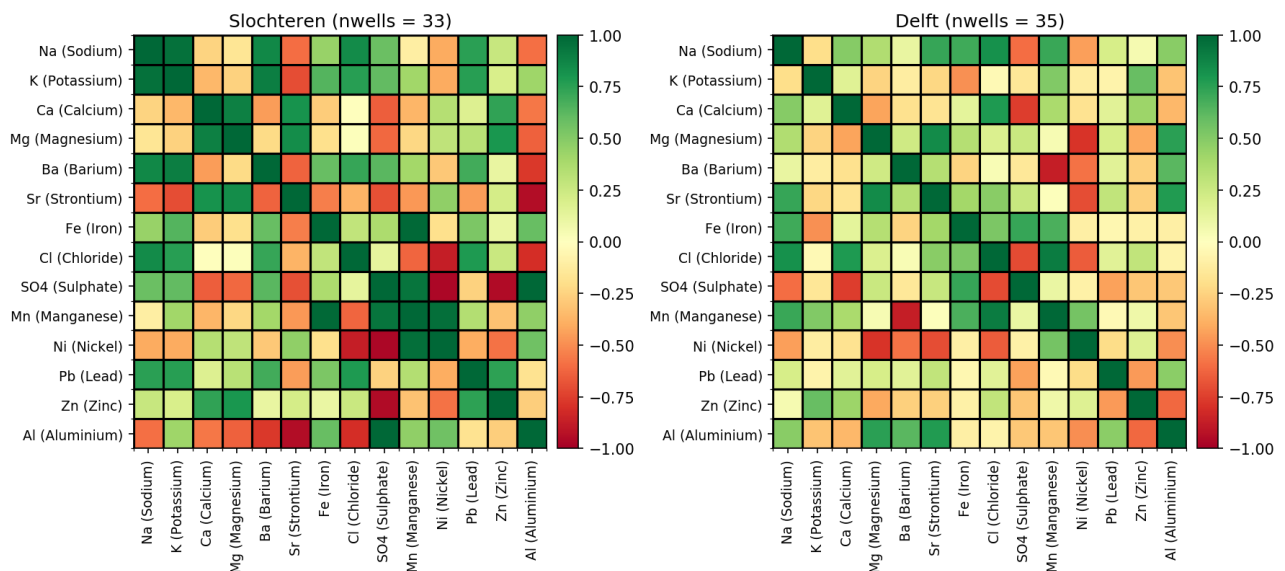


Figure 6.13 Correlation analysis of formation water compositions of the Slochteren reservoir and Delft sandstone reservoir

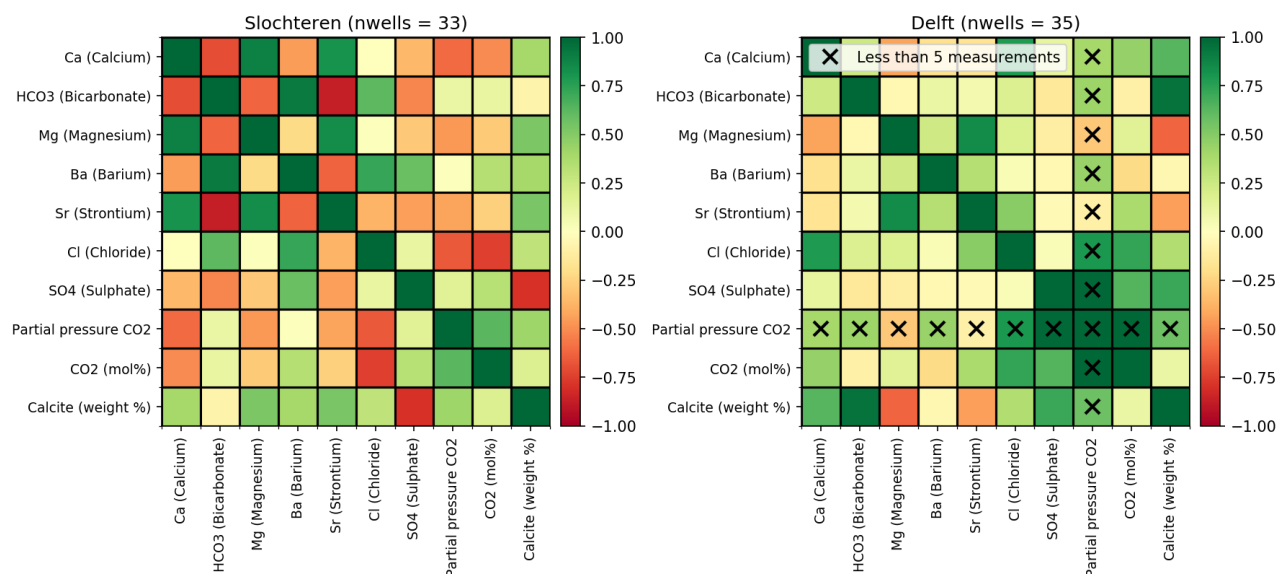


Figure 6.14 Correlation analysis of scaling parameters for the Slochteren reservoir and Delft sandstone reservoir

What makes these correlation analyses difficult to interpret is also the natural variability which is occurring in the formation water and which is hard to constrain. This is shown in Table 6.1 where for each element the average, minimum value, maximum value and standard deviation is calculated. Especially the standard deviation demonstrates the huge variation in the data with for example a standard deviation of 1253.2 mg/l for calcium, where the average is 4689.8 mg/l. This is a deviation of 27% which is very large. In the Delft sandstone data, elements with extremely high standard deviation percentages are observed. For example, potassium with 262% and sulphate with 222%. This happens when the standard deviation is larger than the average value.

Table 6.1 Average, minimum, maximum and standard deviation for each element in the formation water data

Delft sandstone reservoir	Na (Sodium)	K (Potassium)	Ca (Calcium)	Mg (Magnesium)	Ba (Barium)	Sr (Strontium)	Fe (Iron)	Cl (Chloride)	SO4 (Sulphate)	Mn (Manganese)	Ni (Nickel)	Pb (Lead)	Zn (Zinc)	Al (Aluminium)
Average	33958.7	7411.6	4689.8	907.1	18.4	359.4	42.2	67256.6	209.6	1.4	0.4	2.3	0.5	12.9
Min	7752.0	163.2	353.0	240.0	4.2	200.0	0.5	13730.0	49.0	0.9	0.0	0.0	0.0	0.0
Max	46339.7	92818.4	8300.0	1133.0	94.0	444.6	111.0	85000.0	2469.0	2.0	2.0	13.0	1.7	29.5
Standard deviation	7785.6	19385.2	1253.2	179.0	17.4	63.9	31.5	14574.7	464.4	0.4	0.6	3.8	0.5	13.7
Standard deviation %	23	262	27	20	95	18	75	22	222	27	162	164	95	106
Slochteren reservoir	Na (Sodium)	K (Potassium)	Ca (Calcium)	Mg (Magnesium)	Ba (Barium)	Sr (Strontium)	Fe (Iron)	Cl (Chloride)	SO4 (Sulphate)	Mn (Manganese)	Ni (Nickel)	Pb (Lead)	Zn (Zinc)	Al (Aluminium)
Average	64302.4	1393.9	9800.5	1357.7	4.7	414.2	141.3	132136.0	438.1	11.3	1.7	2.0	18.1	7.2
Min	43000.0	650.0	7200.0	1050.0	3.1	250.0	26.3	86000.0	185.0	6.4	0.1	0.4	5.5	0.6
Max	87000.0	2400.0	16600.0	2210.0	6.3	652.6	730.0	160000.0	610.0	29.0	25.0	3.1	49.0	16.0
Standard deviation	15018.9	667.5	3355.8	364.2	1.0	116.5	127.6	23432.2	105.2	5.3	5.7	1.1	12.2	5.1
Standard deviation %	23	48	34	27	21	28	90	18	24	47	342	54	67	72

It has become clear that even though the CO₂ concentrations do appear to correlate to the different reservoirs, the overall variability of the data is very extreme (Table 6.1). This can be caused by natural variability but could also be the result of different lab procedures or analysis techniques. The difficulty is that the reports from the labs that performed the analyses do not state the exact method and that sometimes the original report is not even part of the delivered documents. Another issue is

that for some elements the data density is very low (<5 data points), which makes the results even more unreliable.

A next step could be a very thorough quality control of the dataset, eliminating elements with low data density or unreliable sources. What would also help is more data, which might be difficult in this case since the data is often confidential and hard to come by.

6.3 Thermodynamic calculations

Geochemical speciation codes allow calculation of the saturation state (Ω):

$$\Omega = \frac{IAP}{K_{sp}} = \frac{(X)_{Ac}(Y)_{Ac}}{(X)_{Eq}(Y)_{Eq}},$$

where K_{sp} refers to the solubility product, which gives the equilibrium activities of the ions that form the solid (i.e., $(X)_{Eq}$ and $(Y)_{Eq}$ in the equation above) and IAP, to the product of the actual activities ($(X)_{Ac}$ and $(Y)_{Ac}$). Precipitation of solids requires supersaturation, i.e., $\Omega > 1$ or $\log(\Omega) > 0$. In addition, the geochemical calculations readily give the charge balance for the determined composition of the water. Given that solutions must be charge neutral, deviations from charge neutrality allows us to gauge the quality for the datasets we have assembled. Usually, a charge imbalance of $\pm 5\%$ is accepted for data of reasonable quality (Appelo and Postma, 2005).

6.3.1 Methods

In our calculations, we have used the geochemical speciation software PHREEQC version 3.4 (Parkhurst and Appelo, 2013). The software features a variety of databases that employ different schemes for activity corrections and contains different thermodynamic data (e.g., reaction constants and their temperature and pressure dependence). This difference causes variation in results from calculations depending on the choice of database. Therefore, a benchmarking is currently conducted as part of WP2 of the PERFORM project.

From the benchmarking of the databases so far, the Pitzer database, that is currently distributed with the software (Appelo, 2015), performs well for a range of phases and water compositions. Thus, we have used this database in our calculations. It is able to predict correctly the solubility of the two most important phases in this context, calcite and barite, in NaCl solutions at a variety of pressures (P), temperatures (T), and concentrations (C). However, initial results from the benchmarking suggests that predictions of the solubility of the two phases in CaCl_2 rich solutions are substantially less accurate. So far, calculations result in underprediction of calcite solubility in the tested T range 10-60 °C and overprediction of barite solubility above 100 °C. Three sites, Margretheholm, Groß Schönebeck and IJsselmuiden, extract waters with high CaCl_2 concentrations, and results for these sites should be interpreted cautiously.

The number of parameters that have been measured for the solutions vary with the individual dataset. Some datasets, for example, do not feature measured pH. In the calculations, the pH of such solutions was set to 7. Other datasets do not contain analysis of all major ions. To avoid errors associated with such incomplete data, solutions with high ionic strength (above 1) but no analysis for a major element, i.e., Cl^- , were discarded. For some waters, we have data for only dissolved components in the water, but for others, measurements exist of the concentration of dissolved gasses, including CO_2 whose partitioning influence pH. Consequently, two types of calculations have been conducted.

Firstly, the saturation state was calculated for phases whose solubility is largely insensitive to pH variation and gas content. The calculations were performed using conditions resembling those expected after cooling of the waters at the heat exchanger (25 °C and 15 atm). Secondly, calculations were performed for down hole conditions to understand the saturation state of carbonates and sulphates in the formation waters. For these calculations:

1. Datasets with no data for HCO_3^- were discarded.
2. Water and gas data for sites were coupled in the priority:
 - a. Data for water and gas sampled at the same time were paired
 - b. Where sampled at the same depth, but different time, the water and gas samples were paired.
 - c. For samples taken at different time and at the surface, average values of gas compositions were calculated and paired with solution compositions.
3. For samples with no measured T at Groß Schönebeck, the thermal gradient based on linear regression of T vs depth for other samples at the site was used to determine sample T.
4. In the absence of downhole T measurements, the production T at the time of sampling was used.
5. In the absence of measured downhole pressure, the calculated hydrostatic pressure at the average production depth was used.

6.3.2 Results

The charge balance of the datasets for the various solutions is shown in Table A.1 in the appendix expressed as %error:

$$\%error = \frac{\sum Z_i * C_i}{\sum |Z_i| * C_i} * 100\%$$

where Z_i and C_i refers to the charge and concentration of ion i and $\sum |Z_i| * C_i$ to the total charge of the ions. Most datasets for samples have little error in charge balance beyond what can be expected from the analytical uncertainties. However, two datasets possess error of more than $\pm 15\%$, suggesting that the concentration for some of the elements is inaccurate (Sample ID 202, Mont-Blanc-S138 and Sample ID 204, Rothenbrunnen-SSTH). To give an impression of the charge distribution among major ions, examples for the waters from six sites associated with PERFORM is given in Figure 6.15 in the form of Stiff diagrams, which portrays the distribution of charge among the main ions.

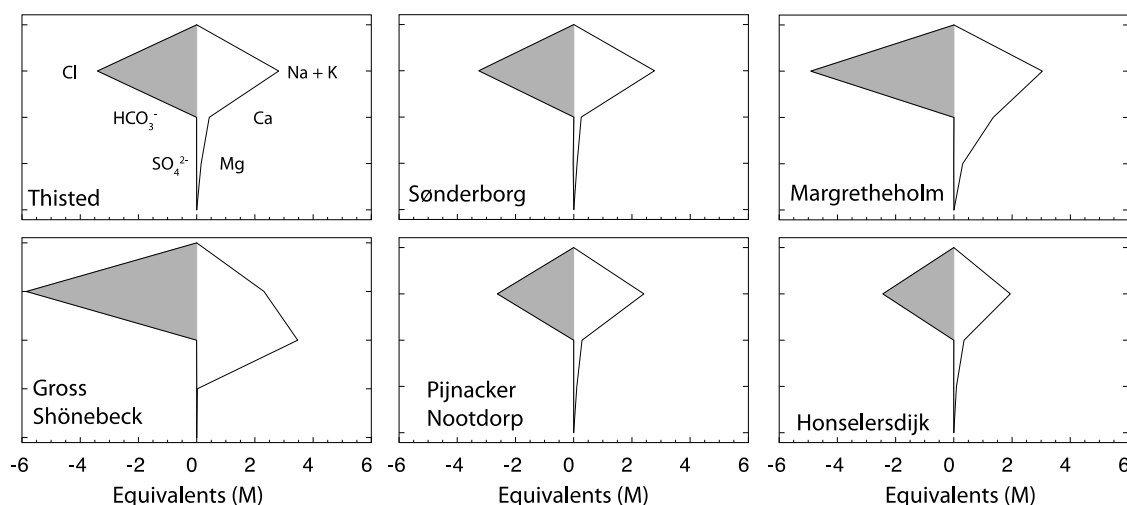


Figure 6.15. Stiff diagram for the waters of 6 sites associated with PERFORM, showing the amount of charge associated with major ions in moles of equivalents per litre.

Table A.1 in the appendix also gives the calculated saturation state for the datasets at 25 °C and 15 atm expressed as $\log(\Omega)$ for barite, celestite, gypsum, halite and amorphous silica. For many of the waters, the phases are undersaturated (i.e., $\log(\Omega) < 0$). Barite, however, is typically supersaturated, with $\log(\Omega)$ reaching almost 2 for a couple of sites (Figure 6.16A). Of the sites that features the highest saturation, evidence for barite precipitation exists downhole at Groß Schönebeck, and at the surface at GeneSys Horstberg, and to minor extend, for stagnant surface waters at Margrethholm (database, Regenspurg et al., 2015, Schulz, 2009). In addition, anonymous sites of the Upper Rhine Graben are reported to be plagued by barite scales (Haas-Nüesch et al., 2018). Quite likely, Insheim is among the sites sampled in this study. For these sites, calculations yield $\log(\Omega) > 1$ for at least some solutions. Caution should be display when interpreting the results, because of uncertainties in the calculations and because precipitation may have affected the composition of the solution both prior and during sampling. Nevertheless, the data suggests that sites producing solutions with $\log(\Omega) > 1$ should be aware that an elevated risk exists for barite scaling (marked by grey area in Fig. 6.16A). At lower supersaturation, slow nucleation kinetics of barite most likely means that significant barite scale will not form.

The results of calculations downhole in wells including the influence of dissolved gasses is shown in Table A.2 in the appendix. Figure 6.16B illustrates the results for datasets where CaCl_2 concentrations and temperatures are such that calculations should be reliable. For most sites, the calculations yield $\log(\Omega)$ close to 0 for barite and/or calcite (i.e., with average values deviating from 0 by less than ± 0.3 unit), suggesting that the formation waters are at equilibrium with one or both of the phases. Exceptions from equilibrium include the dataset from Den Haag, where the formation water is predicted to be substantially supersaturated with respect to barite, and one of the datasets from Thisted Varmeforsyning and from Honselersdijk, where formation waters are indicated to be significantly undersaturated with respect to calcite. Why these datasets are outlying is currently unknown, but we note that the gas concentrations in the two datasets from Thisted Varmeforsyning and from Honselersdijk differ from the other dataset(s) from the sites.

Taken together, the geochemical calculations indicate that many geothermal sites produce from formation waters that are in equilibrium with barite and/or calcite. The solubility of barite decreases with decreasing T and P, meaning that the thermodynamic drive for precipitation is higher after cooling at the surface, i.e., the saturation indices are higher at the surface after cooling as we observe.

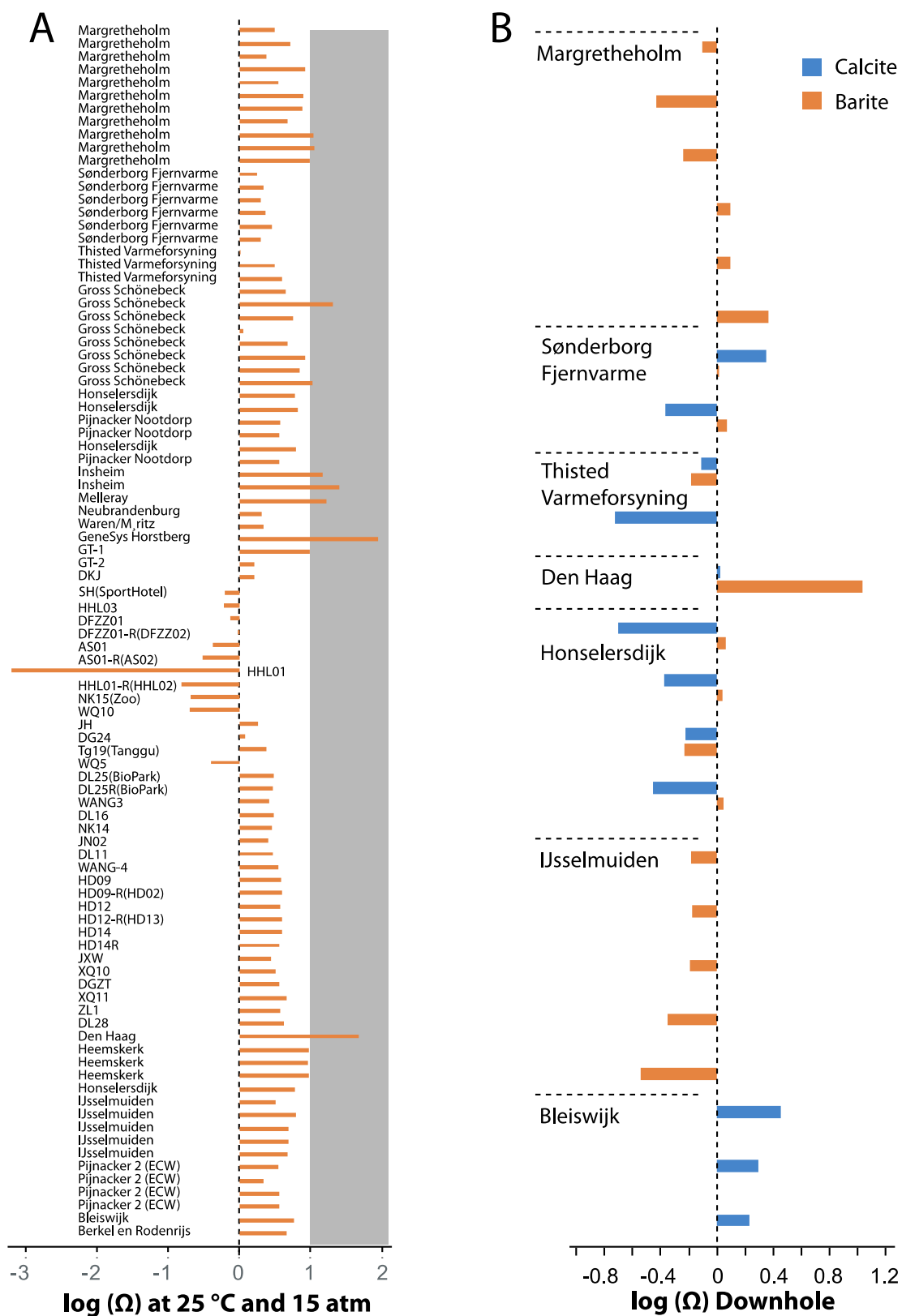


Figure 6.16 A. Saturation indices for barite at 25 °C and 15 atm. B. Downhole saturation indices for barite and calcite

7 Discussion

A database is no better than the quality of the individual datasets it consists of. In our analyses of the data, we have applied several tools that allow detection of anomalous data. The principal component analysis, which allows the detection of outliers within datasets from the same site, generally shows agreement for the determined chemical compositions. Similarly, the calculated charge balance for the datasets is acceptable apart from two datasets. The principal component analysis does provide evidence for some dilution and/or evaporation for samples taken at Groß Schönebeck and a few additional sites. In support of this interpretation, the correlation analysis shows that concentrations of elements at Groß Schönebeck are positively correlated broadly across the datasets as would be expected from dilution. Manual inspection of the concentrations of elements and ions in the Groß Schönebeck dataset suggests that the degree of dilution is fairly small, and not detrimental for the use of the datasets. Due to the very high salinity of fluids in Groß Schönebeck (265 g/L), analysis of samples is very challenging. Brine samples have to be highly diluted before analysing with ICP.

For the production data, machine learning techniques identified anomalies in some of the sensor measurements at the Sønderborg site. It is our hope that the amount of data in the database will grow. Thus, in time machine learning techniques might be applicable to the part of the database containing chemical compositions. Overall, the techniques we have applied to analyse the contents of the database indicates that the vast majority of data is untainted by substantial errors and that it can form the basis for sound interpretations, albeit the uncertainties associated with the challenges of intact sampling of hot, pressurised fluids should be kept in mind.

7.1 Scaling

Precipitation of minerals (scaling), typically observed in installations of geothermal sites, represents a common problem during geothermal exploitation (Boch et al. 2017, Hartog, 2015; Schreiber et al., 2016). Scaling is related to disturbance in the chemical balance, e.g. as a result of temperature or pressure change (and potential gas exsolution) or because of mixing. Scaling can affect both the productivity and injectivity, as the scaling products may result in clogging of the surface installation, wells, perforations or pores of the reservoir rock (Ungemach, 2003, Blöcher et al., 2016, Gallup, 2009, Hessauss et al. 2013). The scaling material is commonly consisting of iron compounds (sulphides, oxides), carbonates (e.g., calcite, aragonite), sulphates (e.g., barite), and at high salinity, chlorides (e.g., laurionite, halite) (Regenspurg et al., 2015).

The correlation analysis of water compositions show that Ba is generally negatively correlated with SO_4 . This is most clear for sites producing deeper seated, saline waters (plot of the correlation in Figure 7.1). Similarly, a negative correlation exists for Ca concentration and the concentration of the CO_3^{2-} ion calculated from the measured pH and HCO_3^- concentration and the equilibrium reaction:



Making the rough assumption that concentrations and activities are equal, the CO_3^{2-} concentration can then be calculated as:

$$[\text{CO}_3^{2-}] = 10^{-10.3} * [\text{HCO}_3^-] / [\text{H}^+]$$

where brackets denote activities.

Albeit the plots do not take activity corrections into account, the samples align with a slope similar to the line representing water-solid equilibrium at far from equilibrium, where activities equal concentrations. This observation imply that the concentrations of the ions have at some point been influenced by dissolution and or precipitation of barite and calcite so that solutions approached

equilibrium. Similarly, thermodynamic calculations indicate that calcite and/or barite are at equilibrium in the formation waters at many sites. Consistent with these analyses, the X-ray diffraction data we have collected for material from the formations also shows the presence of calcite. Barite was not detected with this technique, most likely because it is present in amounts beneath the detection limit of XRD.

The solubility of calcite increases with decreasing temperature, meaning that cooling the water would not increase the thermodynamic drive for precipitation. However, degassing of carbon dioxide ($\text{CO}_{2(g)}$) increases the calcium carbonate saturation, driving the reaction below to the right.



This means that formation of bubbles as pressure decreases when solutions rise in the production well can cause precipitation of carbonate scales. In our database, chemical analysis of sampled solids regularly yields significant Ca concentration, and for several of the datasets, bubbling was reported during the dissolution of the material as would be expected if carbonate minerals were present. Thus, calcium carbonate most likely forms in many plants. For the Pijnacker-Nootdorp site, calcite (and iron carbonate) scaling has been observed within the surface facilities in the first year of production when the installation was operated under lower pressure (personal communication, Wasch et al., 2019). The scaling was related to a high CO_2 content dissolved in the formation brine which outgassed in the gas separation tank. In order to prevent the precipitation of carbonates, the operator has increased the reservoir pressure from 2 to 5 bar, which causes less CO_2 degassing, maintains a higher pH of the geothermal water and prevents scaling. This specific case highlights the possibilities of optimizing geothermal operations to prevent scaling and the power of numerical tools in designing better operational strategies (Wasch et al., 2019).

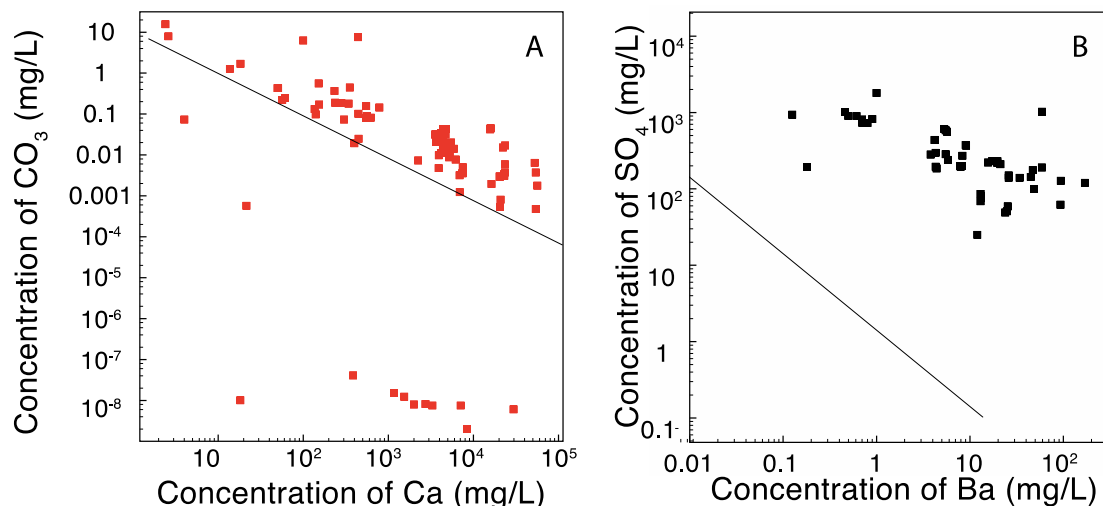


Figure 7.1. A) The correlation between Ca and calculated CO_3 concentration for all datasets with measured Ca, HCO_3 and pH and B) between Ba and SO_4 concentration excluding the low salinity datasets from China (right). Lines denote the solubility of calcite and barite at infinite dilution.

Barite solubility decreases with decreasing temperature. For this mineral, cooling of water at the surface decreases solubility and increases the driving force for precipitation. For solids to form they must, however, first nucleate which requires a threshold value for saturation index to be overcome (e.g., Vekilov 2010). Calculations for an oil well indicate that the threshold saturation for nucleation most likely decrease with T, with $\log(\Omega) > 0.5$ resulting in nucleation and growth of barite deep in the well because of mixing of incompatible fluids (manuscript in preparation). The calculations performed

here indicate that the threshold $\log(\Omega)$ value for nucleation is substantially larger at 25 °C, most likely exceeding $\log(\Omega) = 1$. This threshold value is very poorly defined and its dependence on solution composition is unknown.

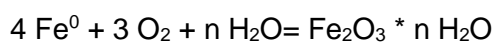
In addition, thermodynamic calculations are uncertain in CaCl_2 rich solutions. For barite, this most likely represents inadequate accounting for the temperature dependence of the stability of the CaSO_4^0 ion pair in the databases. Recent data indicate a decrease in ion pair stability with decreasing temperature by a factor of ~ 3 from 25 to 150 °C (Dai et al., 2015), meaning that the ion pair would to large degree disassociate upon cooling, increasing the concentration of free SO_4^{2-} . If so, this would entail that the barite solubility might be substantially affected by temperature changes in Ca-rich brines, and that sites producing from hot, Ca-rich formation waters are at higher risk for barite scaling. Metal substitution of earth alkalines, such as Ca^{2+} and Sr^{2+} , in barite additionally complicates proper precipitation prediction by modelling. In addition, barite scaling can occur if simultaneous production from separate formations results in mixing of two incompatible fluids.

Based on the analyses of the data in the database we conclude that:

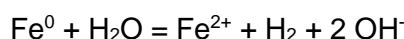
- 1) Calcium carbonate scaling can be largely avoided by maintaining an operational pressure exceeding the bubbling point. The operators of the plants are for most part able to do so. However, geothermal systems with high bubble points or large high temperature geothermal plants might require additional calcite scale prevention measures.
- 2) In general, barite precipitate upon cooling. Barite scaling might, however, be more likely to form at sites that produce water from hot, Ca-rich brines. In addition, the scaling risk could be enhanced at sites that produce from several formations whose minerals have very different chemical compositions, which could yield incompatible waters.
- 3) If threshold $\log(\Omega)$ values for nucleation were better defined and if calculations of saturation states were accurate for a broader range of solution compositions (i.e., in Ca-rich brines), we foresee that the extend of barite formation could be predicted. If formation water composition and temperature can be estimated prior to drilling, risks might even be assessable beforehand.

7.2 Corrosion

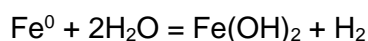
The interaction between brine and metallic elements in the installations at sites commonly results in corrosion, whose reaction products may cause operational problems. Especially sites with steel tubing experience such. Corrosion can occur with a variety of oxidants. It is particularly rapid through redox reaction with oxygen, which cause the formation of Fe oxides (rust) with variable degree of hydration, e.g.:



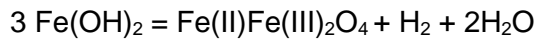
In the absence of O_2 , corrosion occurs anaerobically at much slower rate using water as the oxidant:



This reaction produces hydrogen (H_2). It also increases pH locally so that the solubility of ferrous hydroxide may be exceeded. At such places, the net reaction becomes:



Ferrous hydroxide is not very stable thermodynamically and usually dissolves if pH is not above 7.5 or so. Thus, this material is not able to migrate from the site of formation through the waters in the wells at the vast majorities of the sites where pH is reported. At temperatures above ~75 °C, however, ferrous hydroxide can itself reduce the protons in water at appreciable rates, leading to the formation of the mixed valent iron oxide magnetite, which is thermodynamically very stable:



Thus, formation of smaller amounts of Fe oxides from corrosion of infrastructure with metallic iron is unavoidable. If temperatures are sufficient or oxidation occurs with O₂, the Fe oxides are likely to be thermodynamically stable. The formed Fe oxides are typically nanoparticulate, aggregated to variable degree, and they may migrate with the flow, which could cause clogging of the injection well. Typically, however, they form surface coatings that protect the metallic installations from further corrosion if conditions are not unfavourable. Thus, the slow anaerobic corrosion with water as the oxidant generally causes little harm. The ingress of oxygen, however, can dramatically increase corrosion rates. Hence, the geothermal operations are typically operated at significant overpressure to avoid influx of O₂ (and minimize formation of CO₂).

At the Sønderborg site, which is characterized by moderate salinity and high sulphate concentration, material sampled from the water after cleaning the inside of the injection well consisted of mainly Fe oxides. These may be relict mill scale from the pipe manufacturing that was not properly removed prior to well instalment together with corrosion products that formed during operation. Support of the latter option is given by corrosion monitoring in a side stream loop at the injection well, which shows quite high corrosion rate of steel, and points to oxygen ingress as the main reason. This assessment is based on several independent test methods including corrosion coupons, galvanic probe and ER probe. Analyses of bottom-hole samples show the presence of iron oxides that do not dissolve in lower concentration of acids (1% HCl and 1% HNO₃) as well as higher concentration of acids (5% HCl and 2% HF). Such deposits have also been identified as mill scale in leftover tubing located at the site, suggesting that relict Fe oxide coatings also exists on the installed well tubing. Corrosion taking place in the system could promote the release of the mill scale in the well tubing, allowing the Fe oxides to migrate. Regardless of origin, the Fe oxides may well have accumulated at the sand screens in the injection well or within the gravel pack, contributing to the injection problems at the Sønderborg site.

Samples taken slightly later in the surface installations at the site contained ZnS and PbS, suggesting that sulphate reducing bacteria generate sulphide. Consistent with this, sequencing of DNA from water samples indicates the presence of microorganisms carrying the dissimilatory sulphite reductase gene, albeit they exist in small amounts. Only one type of gene sequence was identified, which is highly related to that of the halophile bacterium *Desulfotomaculum halophilum*. This identification of sulphate reducing bacteria in the infrastructure of geothermal operation echoes findings at other sites, including that at Neubrandenburg (Würdemann et al., 2014), where waters also contains high sulphate concentration (Figure 7.2).

Sulphate reducing bacteria greatly increase anaerobic corrosion rates if present in substantial amounts because the sulphide production destabilizes the passivating Fe oxide coatings (Hamilton, 1985). Thus, their growth can be deleterious to much infrastructure. For the bacteria to thrive, though, several components are needed. An electron donor is needed to reduce sulphate to sulphide. This could be hydrogen present naturally in the environment or produced from anaerobic corrosion of metallic iron in the infrastructure. Based on a limited number of gas measurements, H₂ content may be up to 3.5 mM. If so, H₂ will not limit the bacterial growth. Similarly, the sulphate concentration is high, 700-900 mg/L (Figure 7.2), and would not limit growth either. Potentially, the extend of growth and associated sulphide generation is limited by the availability of assimilable organic carbon, which could mean that microbially induced corrosion rates are fairly low. Methods are available to gauge

the amount of assimilable organic carbon, and if metal sulphides are detected at geothermal sites, it would be prudent to apply them to gauge the potential for microbial growth and the induced corrosion.

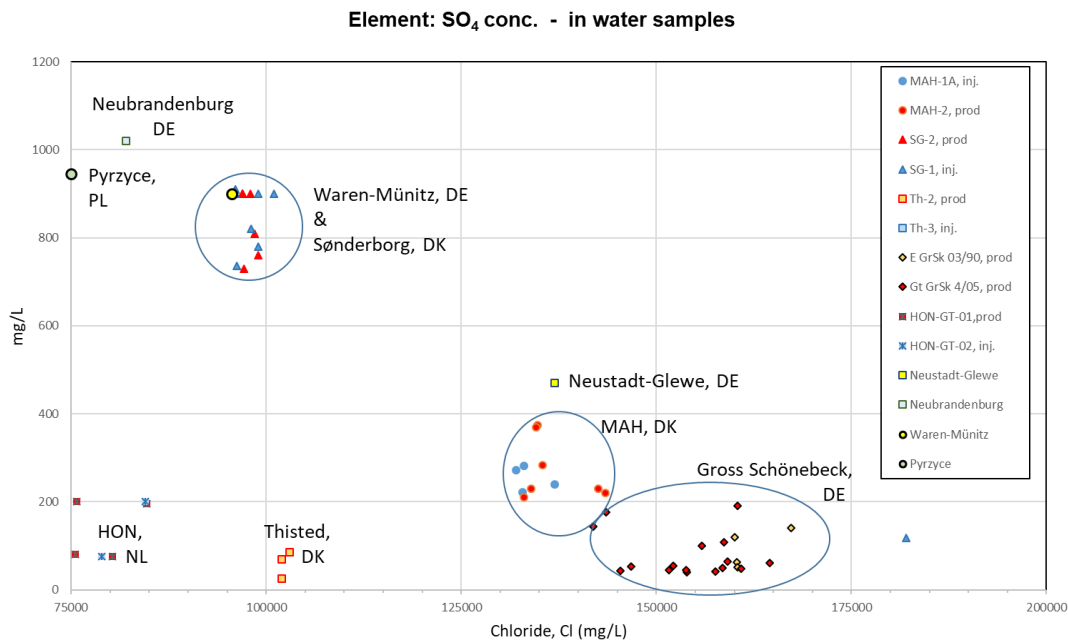
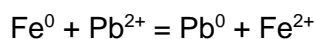


Figure 7.2 Concentration of SO₄²⁻ as a function of chloride concentration.

At the Groß Schönebeck and Margrethelholm sites, analyses in our database of sampled solids display elevated concentrations of Cu or Pb and X-ray diffraction shows the presence of metallic Cu (Cu⁰) or Pb (Pb⁰). The Cu⁰ and Pb⁰ form from corrosion through redox reaction of dissolved metal ions with metallic iron present in the infrastructure, for example:



At the Margrethelholm site, penetrating corrosion of steel has been observed in local areas in the surface installations under influence of high flow, possibly reflecting this type of corrosion (i.e. galvanic corrosion). At Groß Schönebeck, corrosion products of the casing have been observed (magnetite, Fe₃O₄) and hydrogen (H₂) gas has been observed in high concentrations. A corrosion study has been performed over several years. For this purpose, a corrosion test rack was installed as a bypass of the main fluid flow at the site. In the test rack different components and materials were tested for their corrosion behaviour during several years (Saadat et al., 2014). In addition to the Groß Schönebeck and Margrethelholm sites, the open literature indicates that the sites at IJsselmuiden, and Neustadt also suffer from formation of Pb⁰ (e.g., Doornenbal et al., 2019).

The principal component analysis shows that the four sites are among the five sites in the database with the highest score for PC-1. The fifth site, Genesys Horstberg, has not been in proper operation because sufficient amounts of water could not be injected into the formed fractures, meaning that Pb⁰ or Cu⁰ might not have had the time to accumulate to notable quantities at the site. For all operating sites, the corrosion with Cu and Pb as oxidants appears to be systematically related with brine composition and a high score for PC-1 appears to be an indicator for the risk of corrosion at high salinities.

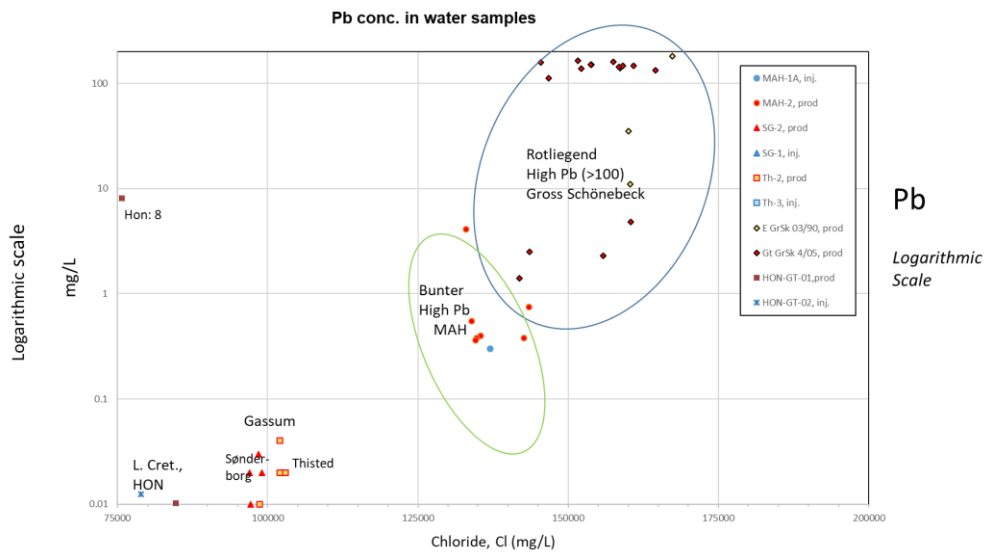


Figure 7.3 Pb concentration as a function of Cl concentration for key sites. Waters are concentrated in Pb in Groß Schönebeck and to slightly lesser extend in Margrethholm (MAH). At Insheim (not shown), the Cl concentration is only 30,000 – 60,000 mg/L (<75,000 mg/L), and the Pb concentration is rather high, c. 1.6 mg/L.

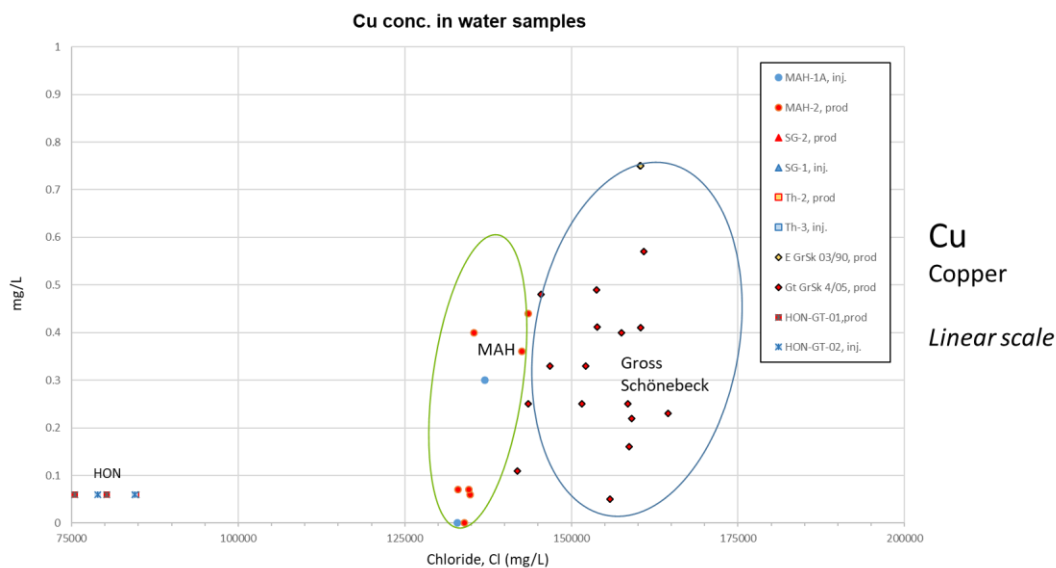


Figure 7.4 Cu concentration as a function of Cl concentration. High concentration of Cu is observed in both Groß Schönebeck and Margrethholm (MAH). At Insheim (not shown), the Cl concentration is only 30,000 – 60,000 mg/L, and the Cu concentration is low, c. 0.024 mg/L.

The correlation analysis shows that Pb and Cl⁻ concentrations are correlated generally (plot in Figure 7.3 for Pb). The same feature applies for Cu (Figure 7.4). Given that i) chloride is an aggressive ion, which generally increases corrosion rates, and ii) rates of reactions typically depend on the concentration of the reactants (in this case the dissolved metal and Fe⁰), the positive correlation of concentrations of the two metals ions and Cl⁻ supports the hypothesis that the extend of corrosion using dissolved metals ions as oxidants might systematically depend on the brine composition. We note that the less saline solution from the Insheim site contain higher Pb concentration compared to Margrethholm (1.6 mg/L versus 0.8 mg/L), but that only limited formation of Pb⁰ occurs at Insheim (assuming that this is indeed the site described by Haas-Nüesch et al. 2018). This indicate that elevated chloride concentrations are required for extensive corrosion. Based on the observations,

we conclude that geothermal plants utilizing highly saline brines operate at elevated risk of corrosion, because the concentration of both chloride and dissolved metals are high, and that this risk should be taken into account when selecting the type of material for the infrastructure.

At the Groß Schönebeck and Margrethesholm sites, the most substantial amounts of Cu^0 and Pb^0 were found on infrastructure in contact with hot water, where reaction kinetics would be generally faster. This effect is supported by the results of corrosion testing of steel in artificial brine, added small amounts of Pb^{2+} . Thus, we propose that the producing well with its hot water is particularly prone to this type of corrosion, whereas the injection well, where cold water is transmitted, should experience the corrosion to smaller extent. Given that the injection well is particularly vulnerable to clogging, this is somewhat encouraging. However, operations in very saline fluids should ensure that filters are adequate, so that particulate Cu^0 and Pb^0 can be removed prior to injection, and waters should not be allowed to pass uncooled through the surface installations into the injection well, which has occurred for some of the sites during testing phases or start up after winter.

The presence of sulphate-reducing bacteria has been observed in the Sønderborg and Pyrzyce sites located in Denmark and Poland, respectively. The bacterial activity generally leads to chemical changes in the geothermal water circuit, resulting in formation of solids and shift in pH. Bacterial activity combined with the presence of an electron donor such as organic material or dissolved hydrogen-sulphide (H_2S) gas in the geothermal water, accelerates corrosion processes and leads to precipitation of sulphide minerals (e.g. ZnS and PbS).

Based on the analyses of the data in the database we conclude that:

- 1) Corrosion by oxygen ingress occurs at high rates and may cause the formation of substantial amounts of Fe oxides that can potentially cause clogging of sand screens in injection wells. Therefore, introduction of oxygen in the geothermal water stream should be avoided. Most operators of the plants are for most part able to do so by maintaining an increased operation pressure.
- 2) Corrosion related to sulphide formation in plants with high sulphate concentrations in the formation water may be a process causing decreased injectivity due to clogging of sand screens with corrosion products. However, the importance of this process is not fully understood and should be subject to future studies.
- 3) Galvanic corrosion by dissolved Pb or Cu seems to be a common problem in geothermal plants where dissolved Pb^{2+} or Cu^{2+} are present in the formation water together with elevated concentrations of chloride. Apparently, the threshold chloride concentration for galvanic corrosion to occur is around 100,000 mg/L, since at geothermal plants with lower chloride concentration and Pb^{2+} in the formation water, galvanic corrosion is only minor. Thus, especially at geothermal with elevated chloride concentrations measures to avoid galvanic corrosion should be taken, either by removing Pb^{2+} or Cu^{2+} from the produced water or by ensuring that the plant infrastructure is constructed of material not prudent to galvanic corrosion.
- 4) Use of improperly cleaned tubings at installation of geothermal wells should be avoided, since e.g. the release of relict mill scale may take place during the operation of the geothermal plant. The release of relict mill scale may potentially be promoted by corrosion.
- 5) Several different corrosion processes may take place in the same geothermal well, resulting in a potential amplification of problems.

8 Conclusions

At the current stage of the PERFORM project, we have succeeded in establishing a knowledge database containing information on operational, chemical and physical aspects of geothermal energy production from a total of 26 geothermal sites across Europe and another ~40 geothermal wells. The amount of data representing each entity in the database varies depending on the data source, varying from detailed information from eight key European geothermal sites to single water analyses from geothermal wells collected from the literature. The database is made available through the PERFORM website.

At the beginning of this project, information on geothermal operations was limited and scattered in the open literature, complicating analysis. The PERFORM database has allowed more reliable data analysis because of the higher amount of data and has also facilitated the comparison of processes and problems observed at individual sites. This is demonstrated in Chapter 6 where various types of analyses were applied to the data; Principal Component Analysis (PCA) and correlation analysis.

Production data from sensors (timeseries) from the Sønderborg wells were analysed using machine learning techniques, which was able to identify anomalies in the datasets and to construct estimates of missing data in series. Given that anomalies in sensor data can indicate the occurrence of processes harmful to the operation, their automated detection is likely to be of value to the operators.

Water composition data were analysed using Principal Component Analysis (PCA), correlation analysis and thermodynamic modelling, and the results were coupled to the information about solids in the database. The data analysis indicates that formation waters often are in equilibrium with calcite and that smaller amounts of calcite typically forms during the geothermal operations, probably because of minor CO₂ degassing. Overall, however, operators are able to manage the calcite scale formation. Many formation waters contain Ba and SO₄ in amounts that indicate down-hole equilibrium with barite. Because the solubility of barite (BaSO₄) decreases with decreasing temperature, such waters become supersaturated after cooling. Nonetheless, the saturation threshold for nucleation is rarely exceeded to a degree that allows barite scale formation. At one site, Groß Schönebeck, substantial amounts of barite forms in the production well. The formation waters at this site are hot and very Ca rich and we propose that the barite formation relates to the significant decrease of the stability of the CaSO₄ ion pair with decreasing temperature.

With respect to corrosion, the analyses indicate that galvanic corrosion with Pb and/or Cu as oxidants poses the largest problem for geothermal operations. This type of corrosion occurs when formation waters are hot and very chloride rich. Our evaluations signify that the chloride concentration should exceed ~100,000 mg/L to maintain extensive corrosion. We interpret that this reflects the aggressive nature of Cl during pitting corrosion and the correlation of the Pb and Cu concentrations in formation waters with that of Cl. For one site, Sønderborg, the installed well tubing most likely contained Fe oxide mill scale from the manufacturing, which was likely mobilised by corrosion from O₂ ingress.

Collectively, the analyses of the data in the database indicate that geothermal exploitation faces a range of (geo-)chemical challenges, but that many of these can be adequately managed by maintaining sufficiently high operational pressure to minimise O₂ ingress and CO₂ degassing. Thus a high operational pressure could limit the encountered scaling and corrosion problems. When waters are hot and Cl rich, however, the exploitation operates at elevated risk of galvanic corrosion in the production well. If such conditions are known beforehand, materials can be selected for the infrastructure to mitigate the problem, e.g. composite casing may be used instead of steel tubing. Alternatively, efficient particle filters could be installed to avoid migration of corrosion products into

the more sensitive injection well and meticulous monitoring of corrosion could allow timely application of corrosion inhibitors or filters for Pb and Cu removal. Such measures should ideally be active at depth in the production well, which complicates their application. High-tech particle and cation filters along with adsorption systems are currently under development within the PERFORM WP3 program.

If waters are also Ca rich, our results indicate that barite scale formation after water cooling becomes likely and that scaling inhibitors or Ba removing filters may be required.

In general, early identification of potential problems and implementation of technical solutions, such as those developed in the upcoming period of the PERFORM project, are of great importance. We believe that continued development and use of the PERFORM knowledge database may broaden our understanding of the challenges faced during geothermal operations and facilitate early stage identification of problems.

Apart from the knowledge database, WP 1 includes data compilation and interpretations. All joining countries have contributed to data collection and the subsequent evaluation of the geothermal data. To our knowledge, geothermal data have not previously been collected and stored in a database at a trans-national level. The set-up of the PERFORM database and website makes it possible to share a comprehensive trans-national dataset, forming the basis of comparing the performance of the different geothermal sites across borders. The data evaluation considers, among other matters, the common scaling and corrosion problems that generally pose a challenge in geothermal exploration. The data in the database - combined with data analyses and discussions on geothermal questions (Chapter 7) - have led to a wider insight into operational issues than could have been achieved from a national point of view. The learnings from the PERFORM database is the start of being able to recognise and possibly mitigate obstacles at an early stage.

References

- Appelo, C. A. J. (2015): Principles, caveats and improvements in databases for calculating hydrogeochemical reactions in saline waters from 0 to 200 °C and 1 to 1000 atm. *Appl. Geochem.* **v. 55**, pp. 62-71.
- Appelo, C. A. J. and Postma D. (2005): *Geochemistry, Groundwater and Pollution*, 2nd Edition. Balkema, Rotterdam. 634 p.
- Baldi, P. (2012): Autoencoders, Unsupervised Learning, and Deep Architectures. In *JMLR: Workshops and Conference Proceedings* (pp. 37–50). <https://doi.org/10.1561/22000000006>
- Bishop, C. M. (2006): *Pattern Recognition and Machine Learning*. Information Science and Statistics. Singapore: Springer Science+Business Media. <https://doi.org/10.1021/jo01026a014>
- Boch, R., Leis, A., Haslinger, E., Goldbrunner, J. E., Mittermayr, F., Fröschl, H., Dietzel, M. (2017): Scale fragment formation impairing geothermal energy production: interacting H₂S corrosion and CaCO₃ crystal growth. *Geothermal Energy*, **5**(1). doi:10.1186/s40517-017-0062-3
- Blöcher, G., Reinsch, T., Henniges, J., Milsch, H., Regenspurg, S., Kummerow, J., Huenges, E. (2016): Hydraulic history and current state of the deep geothermal reservoir Groß Schönebeck. *Geothermics*, **63**, 27-43. doi:10.1016/j.geothermics.2015.07.008
- Bruce, P., & Bruce, A. (2017): *Practical Statistics for Data Scientists (First)*. O'Reilly Media.
- Dai, Z. et al. (2015): A Thermodynamic Model for the Solubility Prediction of Barite, Calcite, Gypsum, and Anhydrite, and the Association Constant Estimation of CaSO₄(0) Ion Pair up to 250 °C and 22000 psi. *J. Chem. Eng. Data* v. 60, pp 766–774.
- Doornenbal et al. (2019): New insights on subsurface energy resources in the Southern North Sea Basin area. In Patruno, S et al. (eds): *Cross-Border Themes in Petroleum Geology I: The North Sea*. Geological Society, London, Special Publications, **v 494**. doi:10.1144/SP494-2018-178
- Erlström M., (2017): *GEOTHERM Project. The Lund Geothermal System. Background, design and review of operational experiences*. Lund University, Department of Geology.
- FORCE Technology, (2017): *GEOTHERM Project. Test plan addressing reduced injectivity*. Report prepared by FORCE Technology, GEUS, Geoop, Hofo, Sønderborg Fjernvarme and Thisted Varmeforsyning.
- Freedman, D., Pisani, R., & Purves, R. (2007): *Statistics (Fourth)*. Norton & Company.
- Gallup, D. L. (2009). Production engineering in geothermal technology: A review. *Geothermics*, **38**(3), 326-334. doi:10.1016/j.geothermics.2009.03.001
- Haas-Nüesch, R. et al., (2018): Mineralogical characterization of scaling formed in geothermal sites in the Upper Rhine Graben before and after the application of sulphate inhibitors. *Geothermics*, **71**, pp. 264–273.
- Hamilton, W. A. (1985): Sulfate-reducing bacteria and anaerobic corrosion. *Annu. Rev. Microbiol.* **v. 39**, pp 195-217.
- Hesshaus, A., Houben, G., & Kringel, R. (2013): Halite clogging in a deep geothermal well – Geochemical and isotopic characterisation of salt origin. *Physics and Chemistry of the Earth, Parts A/B/C*, **64**, 127-139. doi:10.1016/j.pce.2013.06.002
- Kepinska, (2019): Poland Country update. *Proceedings European Geothermal Conference 2019*.
- Lummer, R. & Willert, T., (2019): Innovative fluid system for dissolving lead scales – fluid development and field trial in a geothermal well. In *Proceedings of European Geothermal Congress 2019*.
- Mouchot, J., (2019): Scale and corrosion control program, Example of two geothermal sites in Operation in Upper Rhine Graben. In *Proceedings of European Geothermal Congress 2019*.
- Pastrik, N. and Andrea Förster, (2017): *GEOTHERM Project. Experiences gained from German geothermal plants. A synopsis*. GFZ, Potsdam.

- Parkhurst, D. L. P. and Appelo, C. A. J. (2013): Description of input and examples for PHREEQC. Version 3 – A computer program for speciation, batch-reaction, one-dimensional transport, and inverse geochemical calculations. U.S. Geological Survey, Techniques Methods, book 6, Chapter A43, pp. 1-497.
- Regenspurg, S. et al., (2015): Mineral precipitation during production of geothermal fluid from a Permian Rotliegend reservoir. *Geothermics*, **54**, pp. 122–135.
- Regenspurg, S. et al., (2017): Copper precipitation as consequence of steel corrosion in a flow-through experiment mimicking a geothermal production well. *Geothermal Energy* (2017) **5:11**.
- Schreiber, S., Lapanje, A., Ramsak, P., & Breembroek, G. (2016): Operational issues in geothermal energy in Europe: Status and overview. *The OpERA Magna Carta*.
- Schulz, R. (2009): GeneSys Horstberg II – Methoden und Konzepte zur Erdwärmegewinnung aus gering permeablen Sedimentgesteinen – Zwischenbericht. Leibniz-Institut für Angewandte Geophysik, Hannover, Institut für Geowissenschaftliche Gemeinschaftsaufgaben. 8 p.
- Seibt, P. and Wolfgramm, M. (2008): Reinjection into Sandstone. Problems and Solutions. Workshop for Decision Makers on Direct Heating Use of Geothermal Resources in Asia Tianjin, China, 11 – 18 May 2008.
- Tremosa, J., Marty, N. & Bouchot, V., (2017): Experience with geothermal plants in France. BRGM report prepared for GEOTHERM.
- Ungemach, P. (2003): Reinjection of cooled geothermal brines into sandstone reservoirs. *Geothermics*, **32**(4-6), 743-761. doi:10.1016/s0375-6505(03)00074-9
- Ura-Binczyk, E. et al., (2019): On-site monitoring and laboratory characterization of corrosion processes in the geothermal water of Polish Lowland. *Geothermics*, **77**, pp. 267–277.
- Vekilov, P. G. (2010): Nucleation. *Cryst. Growth Des.* v. 10, pp. 5007–5019.
- Wasch, L., Pejman Shoeibi Omrani, Aris Twerda, (2019): Integrated Scale Management for Geothermal, European Geothermal Conference (EGC) 2019, 11-14 June 2019.
- Würdemann, H. et al., (2014): Influence of microbial processes on the operational reliability in a geothermal heat store – Results of long-term monitoring at a full-scale plant and first studies in a bypass system. *Energy Procedia* v **59**, pp 412-417.

Appendix

Table A.1. Calculated %error and saturation state of solutions at 25 °C and 15 atm expressed as Log(Q) for phases with little pH dependence in solubility

Sample_ID	Site	%error	Barite	Celestite	Gypsum	Halite	SiO2(a)
50	Margrethe-holm	-1.2	0.5	-0.1	-0.5	-0.7	
51	Margrethe-holm	-0.3	0.7	-0.1	-0.4	-0.7	
52	Margrethe-holm	-0.2	0.4	-0.1	-0.4	-0.7	
53	Margrethe-holm	-1.8	0.9		-0.5	-0.7	-0.9
54	Margrethe-holm	-0.9	0.5	-0.1	-0.4	-0.7	
55	Margrethe-holm	-1.8	0.9	0.0	-0.3	-0.7	
56	Margrethe-holm	-1.6	0.9	0.0	-0.3	-0.7	
57	Margrethe-holm	2.7	0.7	-0.6	-0.9	-0.7	
60	Margrethe-holm	-5.6	1.0	-0.2	-0.5	-0.7	
61	Margrethe-holm	-5.2	1.1	-0.2	-0.5	-0.7	
62	Margrethe-holm	-2.2	1.0		-0.5	-0.7	-0.9
63	Sønderborg Fjernvarme	-2.9			-0.4	-1.0	
64	Sønderborg Fjernvarme	-2.4			-0.4	-1.0	
65	Sønderborg Fjernvarme	-2.4			-0.4	-1.0	
66	Sønderborg Fjernvarme	-2.4			-0.4	-1.0	
67	Sønderborg Fjernvarme	-2.3	0.2	-0.1	-0.4	-1.0	
68	Sønderborg Fjernvarme	-2.0	0.3	-0.1	-0.5	-1.0	
69	Sønderborg Fjernvarme	-0.8	0.3	-0.1	-0.5	-1.0	
70	Sønderborg Fjernvarme	-1.1	0.4	-0.2	-0.6	-1.0	-1.1
71	Sønderborg Fjernvarme	-0.2			-2.9	-0.3	
72	Sønderborg Fjernvarme	-1.0			-0.5	-1.0	
73	Sønderborg Fjernvarme	-2.0			-0.5	-1.0	
74	Sønderborg Fjernvarme	-2.3			-0.4	-1.0	
75	Sønderborg Fjernvarme	-2.3			-0.4	-1.0	
76	Sønderborg Fjernvarme	-2.1			-0.4	-1.0	
77	Sønderborg Fjernvarme	-2.3			-0.4	-1.0	
78	Sønderborg Fjernvarme	-1.6	0.5	-0.1	-0.5	-1.0	-1.1
79	Sønderborg Fjernvarme	-1.9		-0.1	-0.5	-1.0	-1.1
80	Sønderborg Fjernvarme	-0.5	0.3	-0.2	-0.6	-1.0	

81	Thisted Varmeforsyning	0.7	0.0	-1.4	-1.8	-1.0	
82	Thisted Varmeforsyning	0.3	0.5	-1.0	-1.4	-1.0	
83	Thisted Varmeforsyning	-0.9				-1.0	
84	Thisted Varmeforsyning	0.0	0.6	-0.9	-1.3	-1.0	
85	Thisted Varmeforsyning	-1.0				-1.0	
99	Gross Schönebeck	-1.8	0.7	-0.3	-0.6	-0.6	
100	Gross Schönebeck	-0.7	1.3	-0.5	-0.7	-0.6	
101	Gross Schönebeck	0.0	0.7	-0.7	-1.0	-0.6	
102	Gross Schönebeck	1.8	0.1	-0.8	-1.0	-0.6	
115	Gross Schönebeck	2.0	0.7	-0.5	-0.8	-0.6	-1.1
116	Gross Schönebeck	6.2	0.9	-0.3	-0.5	-0.7	-1.1
117	Gross Schönebeck	5.3	0.8	-0.4	-0.6	-0.7	-1.1
118	Gross Schönebeck	0.5	1.0	-0.2	-0.5	-0.6	-0.9
132	Honselersdijk	-0.7	0.8	-0.4	-1.1	-1.2	-3.9
133	Honselersdijk	-1.0	0.8	-0.5	-1.0	-1.3	-0.6
134	Pijnacker Nootdorp	3.6	0.6	-0.9	-1.5	-1.2	-4.2
135	Pijnacker Nootdorp	10.6	0.6	-0.9	-1.5	-1.2	-3.8
136	Honselersdijk	-0.7	0.8	-0.4	-1.0	-1.2	-4.2
137	Pijnacker Nootdorp	6.3	0.6	-0.9	-1.5	-1.2	-4.2
161	Insheim	0.7	1.2	-1.1	-1.1	-1.6	-0.1
162	Insheim	0.4	1.4	-0.7	-1.1	-2.2	-0.2
164	Lund	-0.8		-0.8	-1.8	-2.1	-1.2
165	Lund	0.2		-2.2	-3.1	-2.2	-1.2
166	Melleray	-2.1	1.2	-0.1	-0.3	-2.5	
167	Ch,teauroux . St Jean	-0.8			-2.8		
168	Neustadt-Glewe	2.1		0.0	-0.5	-0.5	
169	Neubrandenburg	-2.0	0.3	-0.3	-0.7	-1.2	
170	Waren/-Müritz	0.0	0.3	-0.2	-0.6	-1.0	
171	Neuruppin	0.7		-0.1	-0.3	-0.7	

172	GeneSys	-1.1	1.9	0.8	0.3	-0.3	
	Horstberg						
187	Acquarossa	1.3			-0.1	-8.6	
	-ALB						
217	Pyrzyce	0.8			-0.6	-1.4	
188	Andeer-	0.2			-0.1	-8.9	
	STH						
189	Baden-	3.6			-0.2	-4.7	
	LIMMAT						
190	Bad-Ragaz-	6.2			-2.2	-7.5	
	PFA						
191	Berlingen-	0.8			-2.9	-6.4	
	B3						
192	Bormio-	1.8			-0.5	-8.4	
	SANMA						
193	Brigerbad-	3.1			-0.8	-6.1	
	TQBld						
194	Combioula-	1.1			0.0	-4.9	
	C3						
195	DelÈmont-	4.2			-2.7	-9.1	
	S3						
196	Furka-	-3.7			-2.3	-9.2	
	S8737						
197	Lavey-les-	-1.6			-1.2	-5.7	
	Bains-P600						
198	Leukerbad-	0.8			-0.2	-8.6	
	SANLO						
199	Lostorf-F3	5.7			-0.9	-9.2	
200	Mont-Blanc-	22.0			-2.2	-9.1	
	S138						
201	Riehen-F1	-0.3			-0.1	-3.3	
202	Rothenbrun-	15.4			-1.4	-7.7	
	nen-SSTH						
203	Saeckingen	0.5			-1.6	-4.5	
	-BAD						
204	Saint-	2.8			-0.4	-4.6	
	Gervais-les-						
	Bains-G1						
205	Sankt-	1.1			-0.4	-4.4	
	Moritz-PSG						
206	Schinznach	4.3			-0.6	-6.1	
	-Bad-S3						
207	Simplon-F1	0.0			-0.4	-10.7	
208	Steinenstad	1.4			-1.0	-4.7	
	t-GEORG						
209	Val d'illiez-	3.0			-0.2	-8.7	
	F3						
210	Vals-NB	2.6			-0.2	-9.2	
211	Weissenbur	0.5			-0.3	-8.4	
	g-STH						
212	Yverdon-	2.8			-2.5	-8.3	
	les-Bains-						
	F4						
213	Zurich-B2	1.8			-3.0	-5.9	
214	Zurzach-	2.7			-2.0	-6.0	
	Bad-T1						
215	GT-1	-3.4	1.0	-0.4	-0.6	-5.2	
216	GT-2	2.5	0.2	-1.3	-1.6	-3.8	
218	Podhole	-11.6				-5.2	
219	DKJ	-2.3	0.2	-1.2	-1.1	-5.1	-1.3
220	SH(SportHo-	-2.7	-0.2	-1.4	-1.4	-5.2	-1.4
	tel)						
221	HHL03	4.5	-0.2	-2.6	-2.6	-6.4	-1.6
222	DFZZ01	2.4	-0.1	-2.8	-2.8	-6.1	-1.4

223	DFZZ01- R(DFZZ02)	0.2	0.0	-2.7	-2.6	-6.1	-1.6
224	AS01	-0.7	-0.4	-3.3	-3.1	-6.3	-1.1
225	AS01- R(AS02)	3.7	-0.5	-2.8	-2.9	-6.3	-1.1
226	HHL01	-2.1	-3.2	-6.2	-5.8	-6.9	-1.1
227	HHL01- R(HHL02)	-1.7	-0.8	-3.9	-3.7	-6.9	-1.2
228	NK15(Zoo)	1.6	-0.7	-2.4	-2.5	-5.9	-1.1
229	WQ10	0.7	-0.7	-3.6	-3.2	-6.6	-1.0
230	JH	-1.1	0.3	-1.0	-1.7	-5.1	-1.3
231	DG24	-3.2	0.1	-2.4	-2.6	-5.1	-1.1
232	Tg19(Tangg u)	-3.5	0.4	-1.8	-2.2	-5.4	-0.9
233	Tg19(Tangg u)	0.3			-2.3	-5.4	-0.9
234	WQ5	0.1	-0.4	-3.3	-4.1	-6.4	-0.7
235	WQ5	5.3			-4.1	-6.3	-0.7
236	DL25(BioPa rk)	3.4	0.5	-1.1	-1.6	-5.4	-0.7
237	DL25(BioPa rk)	3.4			-1.5	-5.3	-0.8
238	DL25R(Bio Park)	-1.7	0.5	-1.1	-1.7	-5.3	-0.8
239	WANG3	4.4	0.4	-0.8	-1.8	-6.3	-0.7
240	DL16	-1.5	0.5	-1.0	-1.5	-5.4	-1.1
241	NK14	-4.2	0.5	0.1	-0.1	-4.9	-0.9
242	JN02	-1.1	0.4	-0.9	-1.8	-5.2	-1.1
243	DL11	0.8	0.5	-1.1	-1.5	-5.4	-0.9
244	WANG-4	8.0	0.5	-1.4	-1.7	-6.2	-1.0
245	WANG-4	12.7			-1.7	-6.3	-0.8
246	HD09	-0.9	0.6	-1.1	-1.7	-5.3	-0.8
247	HD09- R(HD02)	-1.3	0.6	-1.1	-1.7	-5.4	-0.7
248	HD12	-2.1	0.6	-1.1	-1.6	-5.3	-0.7
249	HD12- R(HD13)	-0.4	0.6	-1.1	-1.8	-5.3	-0.6
250	HD14	-1.8	0.6	-1.1	-1.7	-5.3	-0.8
251	HD14	-0.5			-1.6	-5.3	-0.7
252	HD14R	-0.2	0.6	-1.1	-1.7	-5.3	-0.7
253	JXW	-0.7	0.4	-1.0	-1.5	-5.1	-1.0
254	XQ10	-2.7	0.5	-1.0	-1.5	-5.1	-0.7
255	DGZT	-1.4	0.6	-1.2	-1.9	-5.2	-0.8
256	DGZT	5.7			-1.8	-5.2	-0.6
257	XQ11	1.1	0.7	-1.1	-1.6	-5.2	-0.6
258	ZL1	5.3	0.6	-1.3	-1.8	-6.2	-0.8
259	ZL1	3.4			-1.7	-6.3	-0.6
260	DL28	-2.7	0.6	-1.1	-1.7	-5.4	-0.9
Hester_1	Den Haag	-0.6	1.7	-0.6	-1.2	-1.3	
Hester_2	Heemskerk	1.5	1.0	-0.1	-0.4	-0.5	
Hester_3	Heemskerk	1.0	1.0	0.0	-0.4	-0.4	
Hester_4	Heemskerk	2.0	1.0	-0.1	-0.4	-0.5	
Hester_6	Honselers- dijk	1.8	0.5	-0.5	-1.0	-1.3	-0.9
Hester_8	IJsselmuide n	-0.5				-0.8	-0.9
Hester_9	IJsselmuide n	2.1	0.7	0.0	-0.3	-0.7	
Hester_10	IJsselmuide n	-6.8	0.7	0.0	-0.3	-0.7	
Hester_11	IJsselmuide n	-1.8	0.7	0.0	-0.3	-0.7	
Hester_12	IJsselmuide n	1.7	0.6	-0.1	-0.4	-0.6	

Hester_13	IJsselmuiden	0.9	0.3	-0.4	-0.7	-0.7	
Hester_22	Pijnacker (ECW)	2 -0.1	0.8	-1.0	-1.6	-1.2	-0.9
Hester_23	Pijnacker (ECW)	2 -0.1			-0.7	-2.8	
Hester_24	Pijnacker (ECW)	2 -0.1				-7.3	-1.5
Hester_25	Pijnacker (ECW)	2 -2.4	0.7	-1.0	-1.7	-1.3	-1.2
Hester_26	Bleiswijk	0.6		-0.6	-1.2	-1.5	-0.6
Hester_27	Bleiswijk	5.1				-1.5	-0.9
Hester_28	Bleiswijk	-1.5		-0.5	-1.1	-1.5	-0.6
Hester_29	Berkel en Rodenrijs			-0.6	-1.1	-1.5	-0.5
Hester_30	Berkel en Rodenrijs					-1.5	-1.2
Hester_31	Berkel en Rodenrijs					-1.4	-1.3
Hester_32	Berkel en Rodenrijs			-0.5	-1.1	-1.4	-0.5

Table A.2. Saturation indices for calcite and barite as well as selected qualities for the solutions at downhole conditions. Numbers in red refers to values that are deemed highly uncertain because of shortcomings in the pitzer database used.

Sample-id	Feature-name	sampling place	T (°C)	P (atm)	Ca (mg/l)	Na (mg/l)	Calcite Log(Ω)	Barite Log(Ω)
51	Margrethe holm	Downhole	73	253	23000	52900	0.5	-0.1
52	Margrethe holm	Downhole	73	253	23100	54000	0.5	-0.4
54	Margrethe holm	Well Head	70	253	23500	53500	0.7	-0.2
55	Margrethe holm	Surface filter before cooling	72	253	22200	52800	1.5	0.1
56	Margrethe holm	Surface filter after cooling	70	253	23600	51300	1.5	0.1
62	Margrethe holm	Well Head	61	253	20505	53974	-0.5	0.4
69	Sønderborg fjernvarme	Well head after cooling	46	110	4600	55900	0.3	0.0
70	Sønderborg fjernvarme	Well Head	46	110	3899	55249	-0.4	0.1
81	Thisted Varme-forsyning	Well Head	37	120	7500	55000	-0.1	-0.2
83	Thisted Varme-forsyning	Well Head	43	120	6909	51882	-0.7	

99	Gross Schönebeck	Downhole	147	446	54000	38400	0.5	-1.6
100	Gross Schönebeck	Downhole	145	435	52500	38150	2.1	-0.8
101	Gross Schönebeck	Downhole	145	432	54000	37900	1.7	-1.4
102	Gross Schönebeck	Downhole	147	436	56500	38700	1.3	-2.2
115	Gross Schönebeck	Downhole	145	434	54000	39200	-0.7	-1.5
116	Gross Schönebeck	Downhole	131	369	53800	39600	-0.8	-1.0
117	Gross Schönebeck	Downhole	122	303	52900	38000	-0.9	-0.9
118	Gross Schönebeck	Downhole	107	238	54800	37700	-0.6	-0.6
133	Honselers dijk	surface (at sideline)	84	263	6190	38800	-0.7	0.1
Hester_1	Den Haag		75	220	5460	39000	0.0	1.0
132	Honselers dijk		84	250	5280	45960	-0.4	0.0
Hester_6	Honselers dijk		84	250	5890	42100	-0.2	-0.2
136	Honselers dijk		84	250	5181	45840	-0.5	0.0
Hester_9	IJsselmuiden		84	189	15850	60350	-0.5	-0.2
Hester_10	IJsselmuiden		84	189	15700	59500	-0.6	-0.2
Hester_11	IJsselmuiden		84	189	16000	61200	-0.4	-0.2
Hester_12	IJsselmuiden		84	189	16300	58900	-0.1	-0.3
Hester_13	IJsselmuiden		84	189	16600	57800	-2.3	-0.5
Hester_26	Bleiswijk		60	175	4370	32700	0.5	
Hester_27	Bleiswijk		60	175	3631	34280	0.3	
Hester_28	Bleiswijk		60	175	4366	33000	0.2	